

1 **A persistent giant algal virus, with a unique morphology, encodes an**  
2 **unprecedented number of genes involved in energy metabolism**

3

4 Romain Blanc-Mathieu<sup>1,2</sup>, Håkon Dahle<sup>3</sup>, Antje Hofgaard<sup>4</sup>, David Brandt<sup>5</sup>, Hiroki  
5 Ban<sup>1</sup>, Jörn Kalinowski<sup>5</sup>, Hiroyuki Ogata<sup>1</sup> and Ruth-Anne Sandaa<sup>6\*</sup>

6

7 1: Institute for Chemical Research, Kyoto University, Gokasho, Uji, 611-0011, Japan

8 2: Laboratoire de Physiologie Cellulaire & Végétale, CEA, Univ. Grenoble Alpes,  
9 CNRS, INRA, IRIG, Grenoble, France

10 3: Department of Biological Sciences and K.G. Jebsen Center for Deep Sea Research,  
11 University of Bergen, Bergen, Norway

12 4: Department of Biosciences, University of Oslo, Norway

13 5: Center for Biotechnology, Universität Bielefeld, Bielefeld, 33615, Germany

14 6: Department of Biological Sciences, University of Bergen, Bergen, Norway

15 \*Corresponding author: Ruth-Anne Sandaa, +47 55584646, [ruth.sandaa@uib.no](mailto:ruth.sandaa@uib.no)

## 16 **Abstract**

17 Viruses have long been viewed as entities possessing extremely limited metabolic  
18 capacities. Over the last decade, however, this view has been challenged, as metabolic  
19 genes have been identified in viruses possessing large genomes and virions—the  
20 synthesis of which is energetically demanding. Here, we unveil peculiar phenotypic  
21 and genomic features of *Prymnesium kappa* virus RF01 (PkJ RF01), a giant virus of  
22 the *Mimiviridae* family. We found that this virus encodes an unprecedented number of  
23 proteins involved in energy metabolism, such as all four succinate dehydrogenase  
24 (SDH) subunits (A–D) as well as key enzymes in the  $\beta$ -oxidation pathway. The *SDHA*  
25 gene was transcribed upon infection, indicating that the viral SDH is actively used by  
26 the virus— potentially to modulate its host’s energy metabolism. We detected  
27 orthologous *SDHA* and *SDHB* genes in numerous genome fragments from  
28 uncultivated marine *Mimiviridae* viruses, which suggests that the viral SDH is  
29 widespread in oceans. PkJ RF01 was less virulent compared with other cultured  
30 prymnesioviruses, a phenomenon possibly linked to the metabolic capacity of this  
31 virus and suggestive of relatively long co-evolution with its hosts. It also has a unique  
32 morphology, compared to other characterized viruses in the *Mimiviridae* family.  
33 Finally, we found that PkJ RF01 is the only alga-infecting *Mimiviridae* virus  
34 encoding two aminoacyl-tRNA synthetases and enzymes corresponding to an entire  
35 base-excision repair pathway, as seen in heterotroph-infecting *Mimiviridae*. These  
36 *Mimiviridae* encoded-enzymes were found to be monophyletic and branching at the  
37 root of the eukaryotic tree of life. This placement suggests that the last common  
38 ancestor of *Mimiviridae* was endowed with a large, complex genome prior to the  
39 divergence of known extant eukaryotes.

## 40 **Importance**

41 Viruses on Earth are tremendously diverse in terms of morphology, functionality, and  
42 genomic composition. Over the last decade, the conceptual gap separating viruses and  
43 cellular life has tightened because of the detection of metabolic genes in viral  
44 genomes that express complex virus phenotypes upon infection. Here, we describe  
45 *Prymnesium kappa* virus RF01, a large alga-infecting virus with a unique  
46 morphology, an atypical infection profile, and an unprecedented number of genes  
47 involved in energy metabolism (such as the tricarboxylic (TCA) cycle and the  $\beta$ -  
48 oxidation pathway). Moreover, we show that the gene corresponding to one of these  
49 enzymes (the succinate dehydrogenase subunit A) is transcribed during infection and  
50 is widespread among marine viruses. This discovery provides evidence that a virus  
51 has the potential to actively regulate energy metabolism with its own gene.

52

53 **Key words:** algal viruses, *Mimiviridae*, persistent, co-evolution, metabolism, energy  
54 production, succinate dehydrogenase,  $\beta$ -oxidation and aminoacyl-tRNA synthetases

## 55 **Introduction**

56 In their essay “Varieties of Living Things: Life at the Intersection of Lineage and  
57 Metabolism,” Dupré and O’Malley proposed to address Schrödinger’s question  
58 “What is Life?” by “*describing a spectrum of biological entities that illustrates why*  
59 *no sharp dividing line between living and non-living things is likely to be useful*” (1).  
60 Microbiologists have contributed considerably to this descriptive effort, both by  
61 reporting the existence of viruses endowed with genes coding for functions once  
62 thought to be exclusive to cellular life and by concomitantly proposing that actively  
63 infecting viruses are a “living form” (2–4). Genes encoding elements for  
64 photosynthesis (5, 6), carbon metabolism (7), and nitrogen- (8) and sulfur-cycling (9)  
65 have been found in bacterial viruses, where they are used to maintain or augment  
66 cellular processes during infection and to redirect energy and resources towards viral  
67 production (8, 10, 11). Genes for protein synthesis, including translation initiation,  
68 elongation, and termination, and a range of aminoacyl-tRNA synthetases have been  
69 found in *Mimiviridae*, a group of giant viruses infecting single-celled eukaryotes (12–  
70 14). *Mimiviridae* and other large DNA viruses, including some bacterial viruses, also  
71 have tRNA genes (15, 16). Ribosomal proteins have recently been reported in viral  
72 genomes derived from metagenomes (17). Genes involved in other metabolic  
73 processes, such as fermentation (18), glycosylation (19), photosynthesis (20), and  
74 rhodopsin (21), are encoded in *Mimiviridae* and other related large eukaryotic DNA  
75 viruses. Metabolic genes are frequently observed within virus genomes (20, 22, 23);  
76 although they represent a tiny fraction of the viral gene pool, these genes have the  
77 potential to dramatically modify the phenotype of an actively infected cell and alter  
78 the ecological role of the host (7, 24, 25). The infected host in this state has been  
79 referred to as a virocell (2). One might expect that the interplay between viral genes

80 and host genes in virocells would become increasingly fine-tuned and complex during  
81 prolonged virus–host co-evolution, which also typically leads to lower virulence.  
82 Much of the complexity of virocells may still be undetected, as most *Mimiviridae*  
83 isolated with their natural host (mostly algae) are highly virulent, with several  
84 involved in rapid algal bloom termination events (26).

85 Viruses of the *Mimiviridae* family are known to infect heterotrophic and  
86 autotrophic microbial eukaryotes. This divide is also reflected in the phylogeny of  
87 these viruses, some of which are classified into two proposed sub-families:  
88 “Megavirinae” and “Mesomimivirinae” (27). The former contains viruses with  
89 genomes larger than 1 Mbp, all isolated from Amoebozoa, while the latter includes  
90 viruses with smaller genomes isolated from haptophyte algae of class  
91 Prymnesiophyceae. Several *Mimiviridae* members outside these two groups have  
92 been characterized to some extent as well, namely, viruses isolated from heterotrophs  
93 (*Cafeteria roenbergensis* virus, CroV; *Bodo saltans* virus, BsV; Choano virus),  
94 autotrophs (*Aureococcus anophagefferens* virus, AaV; Tetraselmis virus 1, TetV;  
95 *Pyramimonas orientalis* virus, PoV; *Prymnesium kappa* virus RF01, PkV RF01), a  
96 metazoan (Namao virus), and metagenomes (Klosneuviruses). The Mesomimivirinae  
97 sub-family includes viruses infecting bloom-forming hosts, such as *Phaeocystis*  
98 *pouchetii*, *Phaeocystis globosa*, and *Prymnesium parvum* (PpV, PgV Group I, and  
99 PpDVAV, respectively) (28–30); it also includes several viruses infecting *Haptolina*  
100 *ericina* and *Prymnesium kappa*, which normally do not form massive blooms but are  
101 present at low densities in seawater year round (31). In marine environments, viruses  
102 infecting low-density and non-bloom-forming algae may be the most common virus–  
103 host systems—that is, low-density hosts (non-blooming) and viruses that appear to  
104 have co-evolved in response to host growth strategy. Thus far, the only known

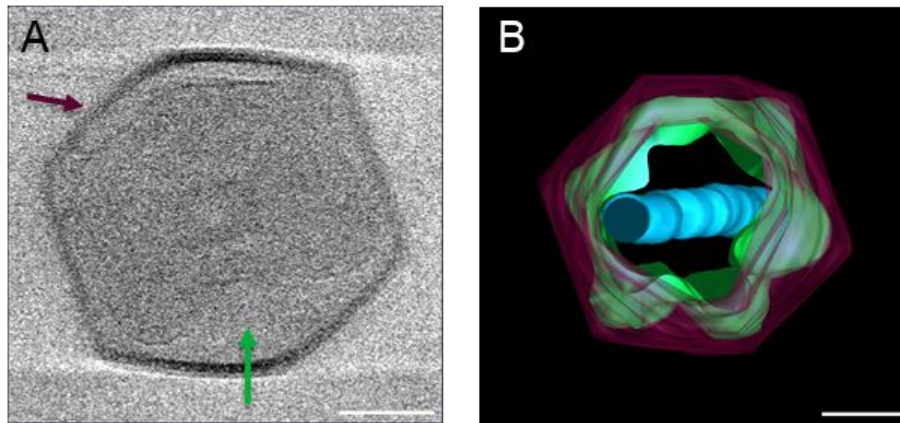
105 representatives of such viruses are *Prymnesium kappa* viruses RF01 (PkV RF01) and  
106 RF02 (PkV RF02), *Haptolina ericina* virus RF02 (HeV RF02), and  
107 *Chrysochromulina ericina* virus (CeV 01B, infecting *Haptolina ericina*) (32, 33).  
108 Together with PgV, all of these viruses, except for PkV RF01, belong to the sub-  
109 family Mesomimivirinae on the basis of their monophyletic relationship and, in the  
110 case of PgV and CeV, a shared genomic similarity (27). In contrast, phylogenetic  
111 analysis of two partially sequenced marker genes has placed PkV RF01 deep inside  
112 the *Mimiviridae* clade, and characterization of its life cycle has revealed an atypical  
113 infection profile (33). Here, we report new phenotypic features as well as new viral  
114 functions inferred from analysis of the genome sequence of PkV RF01. We found that  
115 this virus has a unique morphology, is less virulent than most other alga-infecting  
116 viruses and possesses an unprecedented number of energy-generating genes. We  
117 uncovered clues suggesting that members of *Mimiviridae* that potentially modulate  
118 the metabolism of their hosts are widespread in the ocean. Our findings of peculiar  
119 genomic features in a persistent virus provide new insights on virus–host coevolution  
120 and may stimulate further advances in modeling the history of their interaction.

## 121 **Results and Discussion**

### 122 **PkV RF01 has an atypical morphology**

123 The icosahedral PkV RF01 particle is approximately 400 nm in diameter (Fig. 1).  
124 Beneath the capsid, several convoluted inner membranes fill approximately 66% of  
125 the interior. Treatment of chloroform can be used to identify possible functions of  
126 lipid membranes, as it acts to remove lipid molecules that might be essential for  
127 successful infection (34). Some algal viruses in the NCLDV group are sensitive to  
128 chloroform (30, 35, 36) with the suggestions that lipid containing inner or outer

129 membranes are involved in the infection process (35, 37). In our experiment,  
130 chloroform treatment of PkV RF01 drastically reduced the infectivity of the virus.  
131 ([Appendix – Fig. S1](#)). As no outer membrane was detected by cryo-electron  
132 tomography, the sensitivity to chloroform might be linked to lipid components in  
133 either the capsid or the inner convoluted membranes. Internal lipid-containing  
134 membranes have been detected in several icosahedral-shaped double-stranded DNA  
135 viruses, including algal viruses belonging to families *Phycodnaviridae* and  
136 *Mimiviridae*, mimiviruses, and various bacteriophages (38–43). In all of these viruses,  
137 the inner membranes are suggested to play a role in the release of the viral  
138 nucleoprotein core or genome by fusing with the host plasma membrane (40, 42, 43).  
139 Inner membranes in currently described NCLDVs more or less adopt the icosahedral  
140 morphology defined by the outer layer of capsomers (44, 45). We detected several  
141 convoluted inner membranes in PkV RF01 that do not follow the structure of the  
142 capsid. To our knowledge, this structural inconsistency has not been previously  
143 detected in any double-stranded DNA viruses, which calls for further investigation to  
144 understand the assembly process of PkV RF01 and how it enters its host. Another  
145 striking feature of the PkV RF01 virion is an internal rod-shaped core (ca. 55 nm in  
146 diameter), which is filled with dense material and positioned in the center of the virus  
147 particle. Similar features have been observed in TEM images of large virus-like  
148 particles (VLPs) (300–700 nm) occurring in waste vacuoles of phaeodarian  
149 radiolarians collected from different oceans (46) and in zoospores of the green alga  
150 *Chlorococcus minutum* (47). To our knowledge, however, these features have not  
151 been described in isolated viruses thus far.



152

153 **FIG 1** PkV RF01 morphology. (A) Screen shot of a cryo-electron tomogram of a PkV  
154 RF01 virion. (B) Composite image of 61 cryo-electron tomograms ( $-60$  to  $60^\circ$ ,  
155 imaged every  $2^\circ$ ). Purple, capsid; green, inner membrane consisting of multiple  
156 irregular, convoluted membranes; blue, internal rod-shaped core filled with dense  
157 material. The full set of records is available on GitHub (see [Data availability](#) section).  
158 Scale bar, 100 nm.

### 159 **PkV RF01 has an atypical infection strategy**

160 Only 2% of the total PkV RF01 viral particles produced during infection of *Haptolina*  
161 *ericina* UiO028 (He UiO028) were infectious (able to produce progeny) ([Table 1](#)).  
162 This infectivity was much lower than that of the other two prymnesioviruses, HeV  
163 RF02 and PkV RF02, which produced 13% and 44% of infectious progeny  
164 respectively ([Table 1](#)). The portion of infectious particles of PkV RF01 is low also  
165 when compared to other algal viruses (48, 49). In addition, the latent period of PkV  
166 RF01 was previously reported to be longer (ca. 24–32 h, (33)) in comparison with  
167 other prymnesioviruses (28, 29, 32, 33) and it has been demonstrated that PkV RF01  
168 is also able to infect multi-species (33), that is another unusual trait among algal  
169 viruses (26).

170

171

172



173 **TABLE 1** Infection parameters of *Prymnesium kappa* viruses RF01 and RF02 and  
 174 *Haptolina ericina* virus RF02.

Viral species and hosts	Infectious progeny/mL (MPN)	Host cells/mL (FCM) <sup>a</sup>	Total VLP/mL (FCM)	Burst size (VLP) <sup>b</sup>	Infectivity (%) <sup>c</sup>	Infectious particles in a burst <sup>d</sup>
PkV RF01 (He UiO028)	2.9x10 <sup>6</sup> (± 0.2)	4.9x10 <sup>5</sup>	1.8x10 <sup>8</sup> (±0.9)	363	2	6
PkV RF02 (Pk RCC3423)	2.2x10 <sup>8</sup> (± 0.2)	4.6x10 <sup>5</sup>	5.0x10 <sup>8</sup> (±0.1)	1093	44	483
HeV RF02 (He UiO028)	5.8x10 <sup>7</sup> (±0.2)	4.9 x 10 <sup>5</sup>	4.4 x10 <sup>8</sup> (±0.0)	907	13	119

175 VLP, virus-like particle; MPN, most probable number; FCM, flow cytometry.

176 <sup>a</sup>Measurement performed in duplicates

177 <sup>b</sup>The number of viral particles released from each host cell, estimated from the total number of host cells  
 178 pre-infection and the total number of VLPs produced during the infection cycle.

179 <sup>c</sup>Estimated as the percentage of infectious progeny of all VLPs produced during the infection cycle.

180 <sup>d</sup>Number of infectious particles released per host cell.

181

182 The hosts of PkV RF01, PkV RF02, and HeV RF02 all belong to order the  
 183 Prymnesiales, whose members are normally present in low abundance but co-occur  
 184 year round (*K*-strategists) (50). PkV RF01, PkV RF02, and HeV RF02 are less  
 185 virulent, as shown in the present study, and have longer latent periods compared with  
 186 viruses infecting bloom-forming haptophytes (*r*-strategists). Two of these viruses  
 187 (PkV RF01 and HeV RF02) are also able to infect multi species (generalists) (33).  
 188 Longer replication time and reduced virulence, as hosts becomes scarce, increases the  
 189 chances of vertical transmission rather than horizontal transmission of a virus. As  
 190 vertical parent-to-offspring transmission depends on host reproduction, it has been  
 191 argued that such transmission should select for reduced virulence because the virus  
 192 depend on host survival and reproduction for its transmission (51, 52). High  
 193 virulence, on the other hand, may be supported by large, dense host populations, as  
 194 e.g. algal blooms, because high host densities ensure successful horizontal  
 195 transmission of viral progeny to new hosts (51, 53). Viruses infecting the recurrent  
 196 bloom-forming haptophytes, *Phaeocystis pouchetii* virus (PpV), and *Phaeocystis*  
 197 *globosa* virus (PgV), are indeed highly virulent with between 60%–100% of virus  
 198 particles produced being infectious, resulting in rapid lysis of their hosts (48, 54).

199 Broad host range might also increase the chance of transmission in an environment  
200 with low host abundances (*K*-strategists). Such strategy requires a tradeoff whereby  
201 the virus decreases its opportunity of transmission by evolving longer replication  
202 times, higher decay rates and reduced infectivity (discussed in (55, 56)). This fits  
203 well with our two multi-species infecting haptophyte viruses, PkV RF01 and  
204 HeV RF02, that have reduced proportions of infectious particles and longer  
205 replication times (33), relative to other haptophyte viruses with restricted host ranges  
206 (specialists) like e.g. the *Emiliania huxleyi* virus (EhV), PpV and PgV.

207 The balance between fitness traits, such as virulence, latent period and host  
208 range, and tradeoffs is the result of the adaptive evolution between viruses and their  
209 hosts, resulting in relationships spanning from acute to stable coexistence  
210 (persistence). In the ocean, persistent relationships—such as between PkV RF01 and  
211 its hosts—seem to be most common among viruses infecting unicellular algae; this  
212 has been demonstrated by several metabarcoding studies revealing the persistence of  
213 dominance of viral OTUs over several months (57, 58). The atypical infection  
214 strategy of PkV RF01 evokes a persistent nature, different than the vast majority of  
215 other so far characterized algal viruses.

216

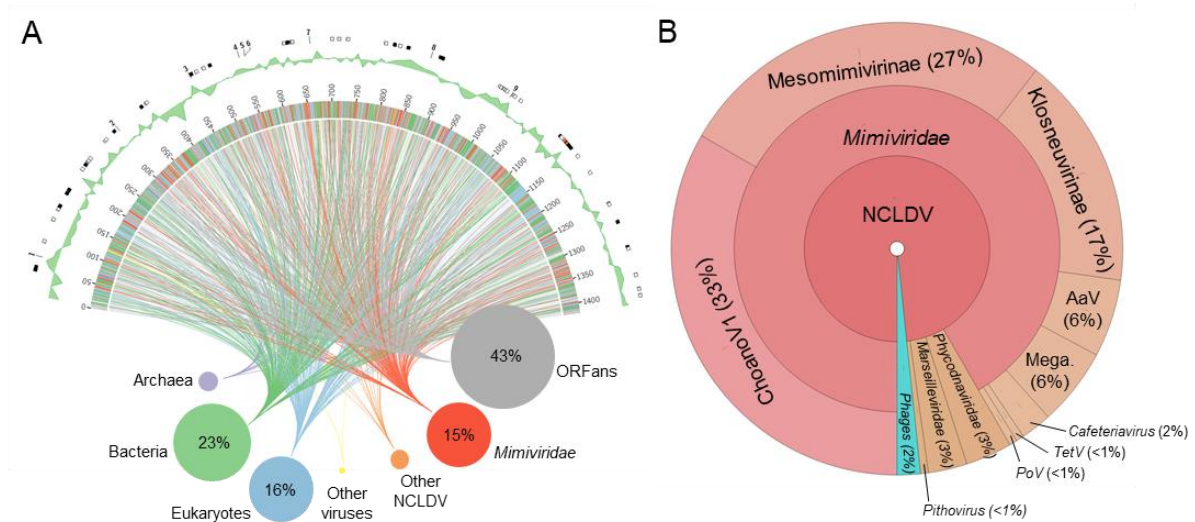
### 217 **PkV RF01 has the largest genome among algal viruses**

218 The genome of PkV RF01 was assembled as a linear DNA sequence of 1,421,182 bp.  
219 This size is more than twice that of the genome of TetV, which means that PkV RF01  
220 has the largest reported genome of any virus infecting a photosynthetic organism (Fig.  
221 2A). Evidence for the linear structure of this genome is the presence of ~5-kbp  
222 terminal inverted repeats. Despite being phylogenetically more closely related to alga-  
223 infecting *Mimiviridae*, the genome size of PkV RF01 is in the range of heterotroph-

224 infecting *Mimiviridae*. The overall G+C content of PkV RF01 is 22.8%, which is low  
225 compared with other *Mimiviridae* (23%–41%). Similar to other *Mimiviridae*, the  
226 average G+C content of PkV RF01 in intergenic regions is relatively low, 17.8%.  
227 This lower G+C content may reflect an ongoing loss of G and C nucleotides, more  
228 prevalent in non-coding than coding regions because of weaker background selection  
229 in non-coding regions. The genome of PkV RF01 is predicted to contain 1,161 genes  
230 comprising 1,121 protein-coding DNA sequences (CDSs) and 40 tRNA genes  
231 corresponding to 13 amino acids ([Appendix – Table S1](#)). Most tRNA genes (30 out of  
232 40) are clustered in three genomic regions that lack predicted CDSs, a feature also  
233 observed in other *Mimiviridae*. For example, all tRNAs of TetV ( $n = 10$ ) and CroV ( $n$   
234  $= 22$ ) are encoded consecutively on the same strand (18, 59). The average CDS length  
235 is 1,046 bp (minimum: 297; maximum: 1,493). Intergenic regions average 217 bp in  
236 length, with a cumulative sum of 244,005 bp, which corresponds to a gene density of  
237 82.8%. Inspection of self-genome alignment dot plots revealed an unusual number of  
238 short repeats throughout the genome of PkV RF01 compared with other *Mimiviridae*  
239 members ([Appendix – Fig. S2](#)).

240         Of the 1,121 predicted CDSs, 641 (57%) exhibited sequence similarities  
241 (BLASTP  $E$ -value conservative cutoff of  $1 \times 10^{-5}$ ) to protein sequences in the  
242 UniRef90 database ([Fig. 2A](#)). Among them, 165 were most similar to *Mimiviridae*.  
243 Curiously, among the CDSs most similar to *Mimiviridae*, sixty were closest to  
244 ChoanoVirus which was isolated from choanoflagellates cultures, followed by  
245 Mesomimivirinae ( $n = 49$ ) and Klosneuvirinae ( $n = 30$ ). ([Fig. 2B](#)). Among the 181  
246 closest homologs found in eukaryotic organisms 23 were haptophytes. A sequence-  
247 based homology search of corrected nanopore reads and scaffolds composing the  
248 initial assembly against *Lavidaviridae* proteomes (BLASTX; matrix: BLOSUM45,  $E$ -

249 value  $< 1 \times 10^{-5}$ ) yielded no significant alignments against any major or minor  
 250 *Lavidaviridae* capsid proteins, which suggests that virophages were absent from the  
 251 sample used for sequencing.



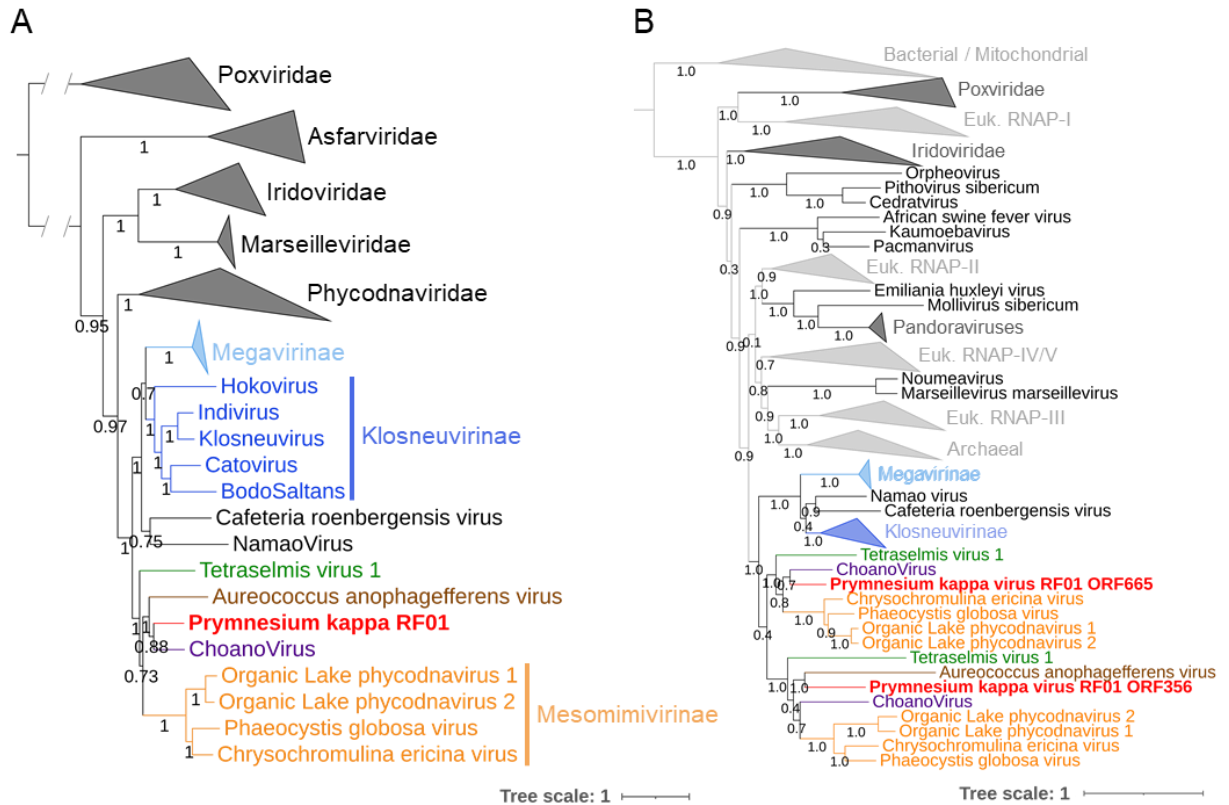
252

253 **FIG 2** Structure and gene taxonomic composition of the PkV RF01 genome  
 254 sequence. (A) Rhizome and genomic features of the PkV RF01 genome. As  
 255 illustrated by the rhizome (inner part of the figure), ORFans comprise the largest set  
 256 of PkV RF01 genes, and a substantial portion (15%) have their best BLAST hits (in  
 257 UniRef90) against “*Mimiviridae*.” Colors indicate taxonomic origin. Intergenic regions  
 258 are white. Percentage hits per taxonomic group higher than 5% of total genes are  
 259 indicated. In the outermost ring, rectangles indicate the positions of  
 260 glycosyltransferases (white), lipid-related enzymes (black), and succinate  
 261 dehydrogenase genes (red), and the numbers correspond to *Mimiviridae* key  
 262 enzymes (1 and 3: DNA-directed RNA polymerase II subunits 1 and 2, respectively;  
 263 2: DNA mismatch repair protein MutS7; 4: Packaging ATPase; 5: VLTF3, 6: Major  
 264 capsid protein; 7: Eukaryotic translation initiation factor 4E; 8: Asparagine synthase;  
 265 9: DNA polymerase family B). The ring adjacent to the outermost ring shows GC  
 266 skew over a 10-KB window. (B) Taxonomic breakdown of 180 genes with best hits to  
 267 virus genes. Mega, Megavirinae; AaV, *Aureococcus anophagefferens* virus; TetV,  
 268 *Tetraselmis* virus 1; PoV, *Pyramimonas orientalis* virus.

269

270 A previous analysis of PkV RF01 family-B DNA polymerase (PolB) and the  
 271 major capsid protein (MCP) placed this virus in the family *Mimiviridae* (33). We also  
 272 recently reported that the PkV RF01 genome has additional NCLDV core genes, such

273 as A32-like virion packing ATPase (NCVOG0249) and RNAPol (RNA pol subunit I  
274 [NCVOG0274] and subunit II [NCVOG0271]), and orthologous genes that are  
275 specific to *Mimiviridae*, namely, MutS7 (NCVOG2626) and asparagine synthase  
276 (AsnS, NCVOG0061) (60). Phylogenetic reconstruction using five NCLDV core  
277 genes confirmed the deep branching of PkV RF01 within the *Mimiviridae* family and  
278 suggested that PkV RF01, along with ChoanoV1, TetV and AaV, is more closely  
279 related to Mesomimivirinae than to Megavirinae (Fig. 3A). In support of this  
280 evolutionary relationship, PkV RF01 has an additional copy of the second largest  
281 RNA polymerase subunit gene (*rpb2*). This *rpb2* duplication is shared with all other  
282 *Mimiviridae* infecting algae, including Mesomimivirinae members, AaV (whose  
283 second copy is very short), and TetV and was previously proposed as a useful feature  
284 to discriminate between the two main clades (autotroph versus heterotroph-infecting  
285 viruses) within the *Mimiviridae* family (27). This additional *rpb2* copy is not found in  
286 other *Mimiviridae* to the exception of ChoanoV1 whose genome was derived from a  
287 single cell metagenome in choanoflagellates cultures. Phylogenetic analysis indicates  
288 that these two *rpb2* copies were present in the ancestor of alga-infecting *Mimiviridae*  
289 and ChoanoV1 (Fig. 3B). In agreement with the five NCLDV core genes phylogeny,  
290 it suggests that PkV RF01 and ChoanoV1, although evolutionarily distant, are more  
291 related with each other compared to any other *Mimiviridae*.



292

293 **FIG 3** Phylogenetic evidence for PkV RF01 as a distant relative of

294 “Mesomimivirinae.” (A) Bayesian phylogenetic tree of NCLDVs reconstructed from a  
295 concatenated alignment of five core nucleocytoplasmic virus orthologous genes.

296 Values at branches are posterior probabilities support. The tree was rooted using

297 *Poxviridae* as outgroup. The scale bar indicates substitutions per site. (B) Maximum

298 likelihood phylogenetic tree of cellular and NCLDV DNA-directed RNA polymerase

299 subunit beta (RPB2). Values at branches are Shimodaira-Hasegawa-like local

300 support. Tools, evolutionary models, and parameters used for tree reconstruction are

301 reported in [Appendix 1 – Table S3](#).

302

303 Out of 1,121 predicted protein-coding genes in the genome of PkV RF01, only

304 about a third could be annotated with some functional description based on their

305 sequence homology with characterized proteins. Such a small percentage is typical of

306 divergent eukaryotic viruses detected for the first time. A total of 339 proteins (30%)

307 showed significant sequence similarity with proteins in the Cluster of Orthologous

308 Gene (COG) database (61) ([Appendix – Fig. S3](#)). The distribution of COG functions

309 associated with these hits was dominated by “Posttranslational modification, protein



310 turnover, chaperones” (43 proteins) and “Cell wall/membrane/envelope biogenesis”  
311 (42 proteins), which is approximately two times more proteins than in other  
312 *Mimiviridae* members except for Tupanvirus ([Appendix – Fig. S4](#)). Among other  
313 well-represented categories, numbers of proteins in “Replication, recombination and  
314 repair” (36 proteins) and “Transcription” (23 proteins) were similar to those of other  
315 *Mimiviridae*, while the categories of “Translation, ribosomal structure and  
316 biogenesis” (25 proteins) and “Amino acid transport and metabolism” (20 proteins)  
317 were respectively in the same range or higher than those of heterotroph-infecting  
318 *Mimiviridae* (mimiviruses, BsV, and CroV). Interestingly, 24, 17, and 9 PkV RF01  
319 proteins were respectively assigned to the categories of “Lipid transport and  
320 metabolism”, “Carbohydrates transport and metabolism,” and “Energy production and  
321 conservation,” all much higher compared with other *Mimiviridae* viruses.

322         Similar to other *Mimiviridae*, PkV RF01 encodes several genes involved in  
323 DNA repair, transcription, and translation ([Appendix – Results](#)). Notably, this virus  
324 has the full set of enzymes required for the base excision repair (BER) pathway,  
325 which is also the case for all *Mimiviridae* members except for those with smaller  
326 genomes (PgV, CeV, and AaV). PkV RF01 BER enzymes are closer (i.e., have a  
327 greater alignment score) to heterotroph-infecting *Mimiviridae* than to cellular  
328 homologs, thus suggesting that this pathway was present in the last common ancestor  
329 of *Mimiviridae*. According to a previous phylogenetic analysis, *Mimiviridae* BER  
330 enzymes are monophyletic with regard to *Mimiviridae* and have not recently been  
331 acquired from eukaryotes (62).

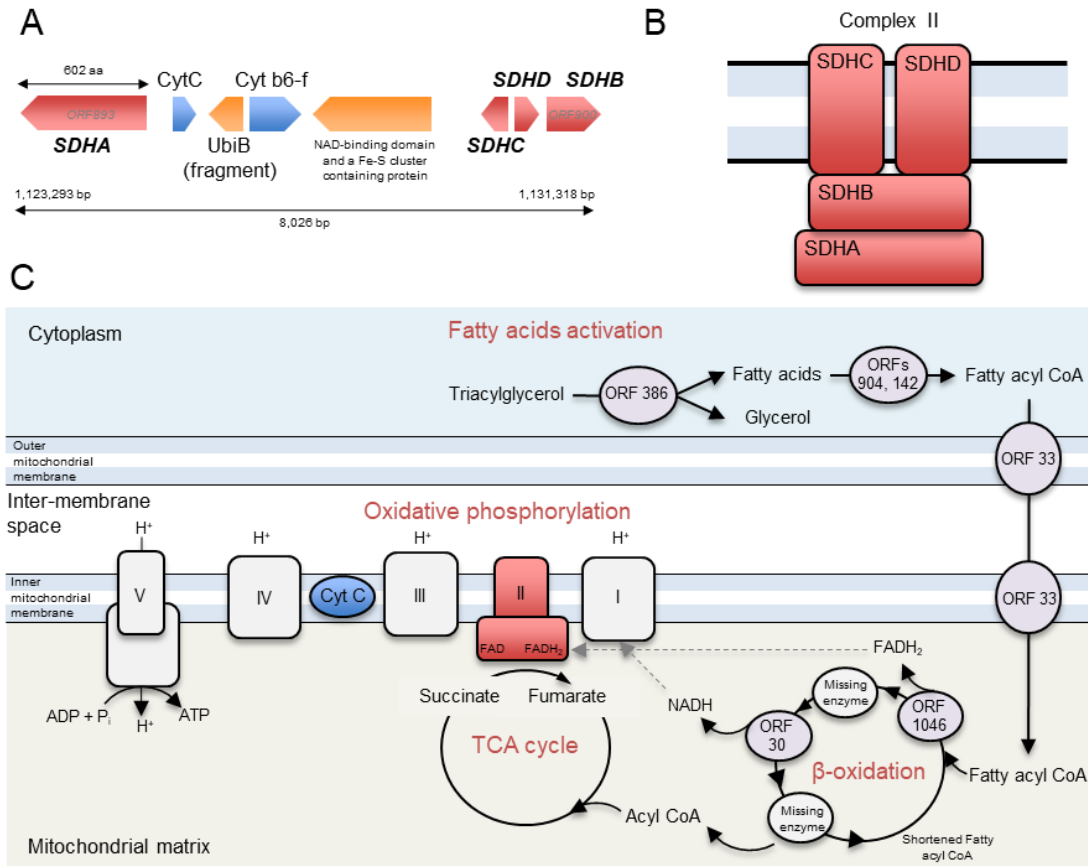
332         Unlike alga-infecting *Mimiviridae*, PkV RF01 encodes two amino-acyl tRNA  
333 synthetases (aaRS): an isoleucyl-tRNA synthetase (IleRS; ORF 480) and an  
334 asparaginyl-tRNA synthetase (AsnRS; ORF 764). Both of these synthetases are found

335 in most lineages of heterotroph-infecting *Mimiviridae* (AsnRS is missing from CroV  
336 and BsV, and IleRS is missing from *Mimivirus* lineage A). Phylogenetic analyses of  
337 these two proteins revealed a deep branching of viral homologs, which formed a  
338 monophyletic clade well separated from cellular homologs ([Appendix – Fig. S5 and](#)  
339 [Results](#)).

#### 340 **A viral-encoded succinate dehydrogenase and energy production genes**

341 We found six predicted protein-coding genes (ORFs 893 to 900) related to energy  
342 production in an 8,026-bp region ([Fig. 4A](#)). Four ORFs (ORFs 893 and 898–900)  
343 were predicted to code for all four subunits (SDHA, D, C, and B) of a functional  
344 succinate dehydrogenase (SDH, or Electron Transport Chain Complex II) of the  
345 oxidative phosphorylation pathway ([Fig. 4B](#)). In eukaryotes, all four subunits of this  
346 enzyme are encoded in the nuclear genome. This enzyme acts in the mitochondrial  
347 respiratory chain and participates in both the TCA cycle and the respiratory electron  
348 transfer chain. In the TCA cycle, this succinate dehydrogenase oxidizes succinate to  
349 fumarate, while its activity in the inner mitochondrial membrane involves the  
350 reduction of a FAD cofactor followed by electron transfer through three Fe–S centers  
351 to ubiquinone ([Fig. 4C](#)).





352

353

**FIG 4** Genes in PkV RF01 predicted to encode enzymes of oxidative phosphorylation

354

and β-oxidation pathways. (A) Gene organization in the succinate dehydrogenase-

355

containing region. (B) Schematic representation of the canonical enzymatic complex

356

II in the mitochondrial membrane. (C) Location of succinate dehydrogenase in the

357

TCA cycle and electron transport chain as known in plants and a schematic

358

reconstruction of the PkV RF01-encoded β-oxidation metabolic pathway.

359

360

*SDH* genes have recently been reported in viral genomes assembled from

361

environmental samples for which functional experiments cannot be done (63). In a

362

RT-PCR experiment using primers specific for the PkV RF01 gene for *SDHA*

363

(hereafter, *vSDHA*), we detected transcripts of this gene in samples collected 24, 72,

364

and 96 h post infection (Fig. 5). The *vSDHA* primers were tested on an uninfected

365

culture to ensure that only the viral version of the *SDHA* gene was amplified

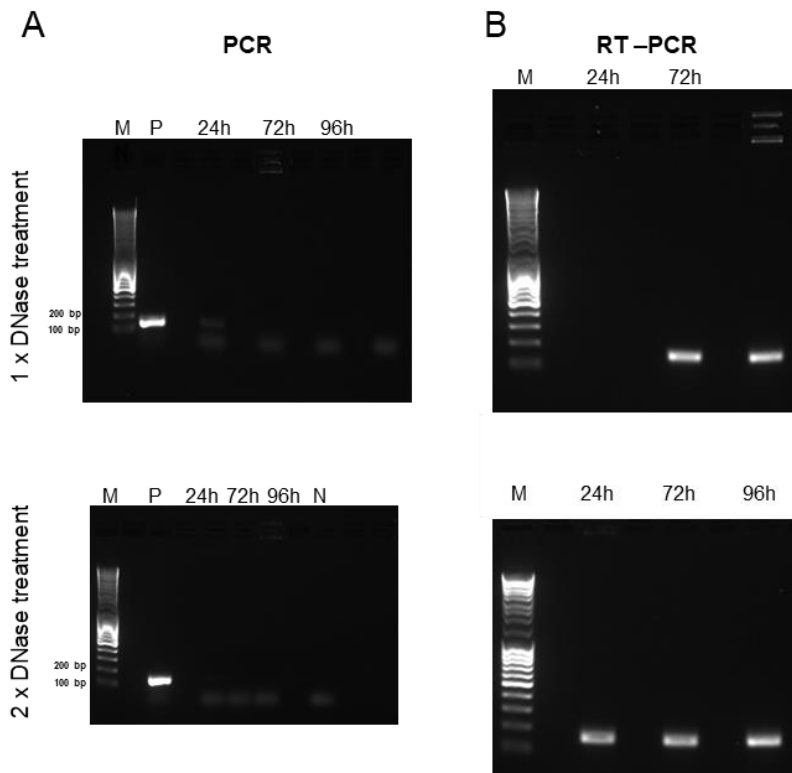
366

(Appendix – Fig. S6). The MCP gene of PkV RF01 was used both for protocol

367

optimization and later as an internal positive control (Appendix – Materials and

368 **Methods; Fig. S7).** Although the transcription of the viral *SDHA* suggests that the  
369 viral SDH is functional, we can only speculate on the possible role of this enzyme  
370 during infection. One possibility is that the viral SDH sustains the carbohydrate  
371 metabolism of infected cells (i.e., virocells) to supply building blocks of viral particles  
372 such as amino acids and to support proper replication of this large virus. Another  
373 possibility is that PkV RF01 uses its SDH as a part of an arms race with its host to  
374 turn on the TCA cycle after the host had turned it off to counter viral replication, or  
375 more simply to boost the energy metabolism of the virocells to augment the fitness of  
376 the host and/or to maximize virus production efficiency.



377  
378 **FIG 5** The viral *SDHA* gene is transcribed during infection. Gels of PCR and RT-PCR  
379 in combination with a TURBO DNA-free kit. Samples were taken 24, 72, and 96 h  
380 after infection. (A) PCR with *vSDHA*-specific primers was used to check for the  
381 presence of genomic DNA after RNA isolation treated with 1x and 2x DNase, in the  
382 upper and lower panels respectively. P, positive control (PKV RF01 genomic DNA);  
383 N, negative control (*sdH<sub>2</sub>O*). (B) RT-PCR of RNA samples using *vSDHA*-specific  
384 primers. M, DNA marker (MassRuler DNA Ladder Mix, Thermo Fisher, 80 to 10,000  
385 bp).

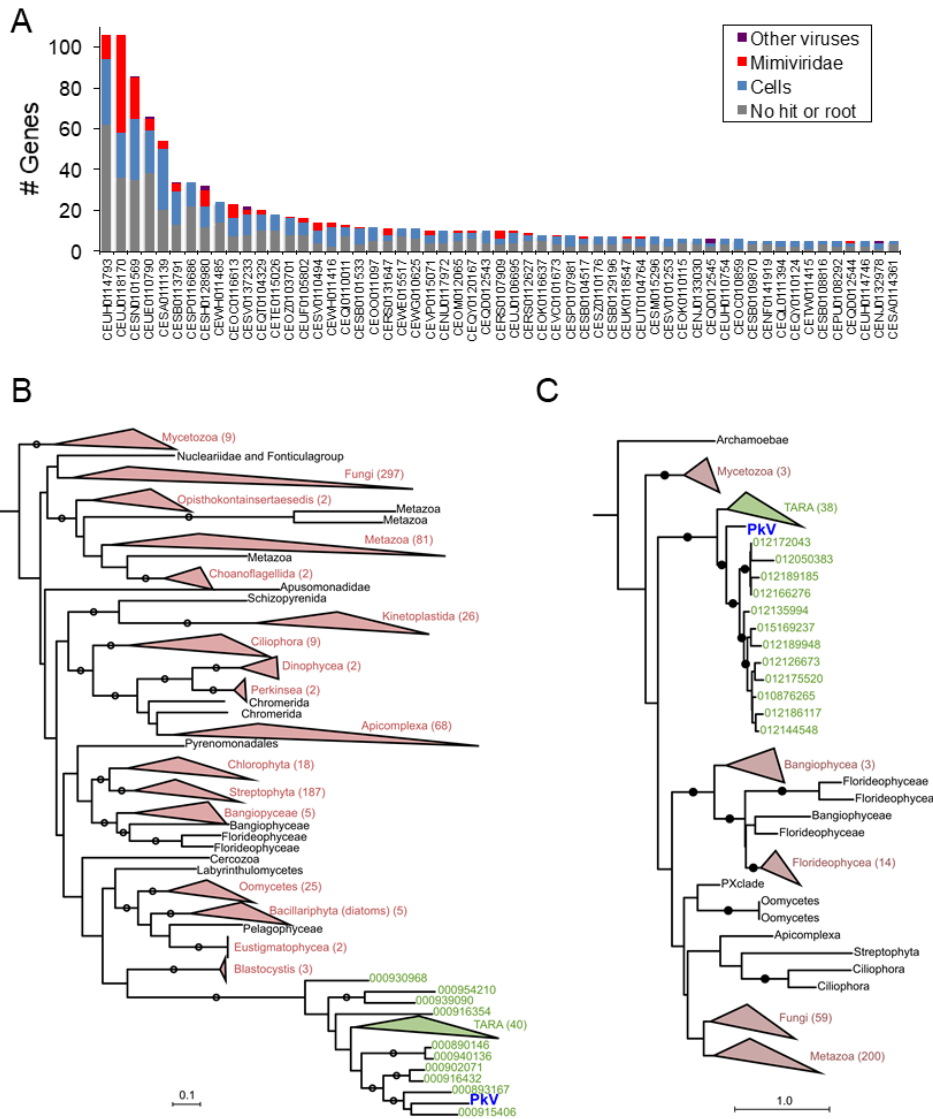
386           The discovery of the viral SDH prompted us to search for other potential viral-  
387 encoded SDHA and SDHB homologs in marine metagenomes. These two subunits  
388 (SDHA and SDHB) form the catalytic core containing the redox cofactors that  
389 participate in electron transfer to ubiquinone; they are thus more conserved than  
390 SDHC and SDHD subunits. To test for the presence of this viral SDH in other viruses,  
391 we searched for *vSDHA* and *B* in marine metagenomes of the *Tara* Oceans  
392 expedition. The 50 most-similar and non-redundant SDHA and B sequences predicted  
393 from 101 *Tara* Oceans genome fragments were most likely derived from *Mimiviridae*  
394 viruses (Fig. 6). Indeed, out of 1,113 genes predicted from these 101 genome  
395 fragments, 681 were annotated at some taxonomic level, of which 449 were predicted  
396 to be cellular and 157 viral. Of the 157 viral genes, 146 and 130 had their last  
397 common ancestor in *Mimiviridae* and *Mesomimivirinae*, respectively. A total of 32 of  
398 the 101-genome fragments contained at least one gene predicted to be of *Mimiviridae*  
399 origin, and the larger the genome fragment, the more *Mimiviridae* genes it was found  
400 to encode (Fig. 6A). Functional analysis indicated that 12 of the 1,113 predicted genes  
401 were NCLDV hallmark genes (encoding five VLTF3s, two capsid proteins, two  
402 PCNAs, two helicases, and one PolB). The high proportion of unknown genes and  
403 genes annotated as *Mimiviridae* in the 101 *Tara* Oceans genome fragments encoding  
404 SDHA or SDHB strongly suggests that these fragments belong to *Mimiviridae*  
405 viruses. This finding demonstrates that the presence of SDH is not restricted to PkV  
406 RF01 and is arguably widespread among marine *Mimiviridae*. According to  
407 phylogenetic analyses of cellular and viral SDHA and SDHB, the viral homologs  
408 form a monophyletic group that branches deeply within eukaryotic lineages (Fig. 6B-  
409 C). Long-branch attraction bias could generate such topologies but, as explained  
410 above for the IleRS and AsnRS, it is more likely that the viral SDHA and SDHB were

411 acquired at an early stage in the radiation of eukaryotic lineages. The transcription of  
412 *vSDHA* and its occurrence in marine environments calls for further investigation to  
413 understand the biological role and co-evolutionary significance of this viral SDH.

414 Other genes related to energy production were detected in the 8,026 bp-long  
415 region. ORF 894 and ORF 896, respectively corresponding to cytochrome *c* (CytC)  
416 and cytochrome b6-f complex iron-sulfur (Cyt b6-f) subunits, showed high sequence  
417 conservation with *Chrysochromulina* sp. CCMP291 proteins (78% and 59% amino  
418 acid [aa] identities, respectively). CytC is a short protein (~100 aa) involved in the  
419 oxidative phosphorylation pathway, where it accommodates the transfer of electrons  
420 between the coenzymes Q-cytochrome *c* reductase (complex III) and cytochrome *c*  
421 oxidase (complex IV). The presence of Cyt b6-f between oxidative phosphorylation  
422 genes is puzzling because the cytochrome b6-f complex is involved in photosynthesis.  
423 The core of the chloroplast b6f complex, however, is similar to the analogous  
424 respiratory cytochrome bc(1) complex. The other two predicted ORFs in this region  
425 are similar to ubiquinone biosynthesis protein UbiB (ORF 895) or contain a NAD-  
426 binding domain and a Fe-S cluster (ORF 897) and may thus be associated with  
427 electron transport as well. ORF 897 has two distant (25%–31% aa identity) homologs  
428 in the PkV RF01 genome (ORF 456 and ORF 625).

429 Some other genes were predicted to encode enzymes involved in pyruvate  
430 metabolism. ORF 79 has sequence homology with L-lactate dehydrogenases; it might  
431 thus catalyze the conversion of lactate to pyruvate, an intermediary compound serving  
432 as a starting point for several major metabolic pathways, such as glycolysis,  
433 gluconeogenesis, and the TCA cycle. ORF 727 was predicted to code for an  
434 isochorismate hydrolase that also produces pyruvate from isochorismate. ORF 24 and  
435 ORF 726 share sequence homology with phosphoenolpyruvate synthase and a partial

436 pyruvate kinase, respectively. The former catalyzes the conversion of pyruvate to  
 437 phosphoenolpyruvate (PEP), while the latter catalyzes the reverse reaction. Formation  
 438 of PEP is an initial step in gluconeogenesis.



439  
 440 **FIG 6** Origin of PkV RF01 SDHA and SDHB and their most similar homologs in *Tara*  
 441 Oceans metagenomes. (A) Taxonomy of genes predicted in *Tara* Oceans  
 442 metagenome assembled-genome fragments encoding the 50 SDHAs and SDHBs  
 443 most similar to PkV RF01 genes (for genome fragments having at least five predicted  
 444 genes). (B and C) Phylogenetic trees of viral and cellular SDHAs (B) and SDHBs (C).  
 445 Clades in green contain PkV RF01 SDHA or SDHB and their 50 most similar hits  
 446 identified in *Tara* Oceans metagenomes (predicted to be *Mimiviridae* homologs from  
 447 A). Red, eukaryotic phyla; black, unclassified eukaryotes. Trees are rooted with  
 448 Proteobacteria and Firmicutes homologs (not shown). Circles indicate branches with  
 449 posterior probability support  $\geq 50\%$ .

## 450 **A nearly complete viral-encoded $\beta$ -oxidation pathway**

451 In this study, 22 predicted genes were inferred to code for proteins involved in lipid  
452 synthesis or degradation, including key enzymes of the  $\beta$ -oxidation pathway  
453 ([Appendix – Table S2](#)). Several genes were predicted to code for lipase-like proteins  
454 (ORFs 386, 481, 635, 653, and 690), including a triacylglycerol lipase (ORF 386) that  
455 can break down triacylglycerol into glycerol and fatty acids. Glycerol and fatty acids  
456 can be used as a starting point for ATP production—by glycolysis and  $\beta$ -oxidation,  
457 respectively. In the  $\beta$ -oxidation pathway, fatty acids are fully oxidized to produce  
458 acetyl-CoA, which can then enter the TCA cycle to yield NADH and FADH<sub>2</sub>; these  
459 latter two products can funnel through to the electron transport chain to produce ATP  
460 ([Fig. 4C](#)). Each  $\beta$ -oxidation cycle itself also produces NADH and FADH<sub>2</sub> cofactors.  
461 We found that PkV RF01 encodes key  $\beta$ -oxidation enzymes. First, two distantly  
462 related ORFs (ORF 142 and ORF 904 sharing 22% aa identity) have sequence  
463 homology with a long-chain fatty acyl-CoA synthetase. This enzyme catalyzes the  
464 formation of fatty acyl-CoA in the cytosol. Fatty acyl-CoA can be imported to  
465 mitochondria using a (carnitine) CoA-transferase also encoded in PkV RF01 (ORF  
466 33). Once in the mitochondrial matrix, fatty acyl-CoA serves as a substrate on which  
467 an acyl-CoA dehydrogenase (ORF 1046) oxidizes the fatty acyl-CoA and reduces a  
468 FAD cofactor to produce a FADH<sub>2</sub> cofactor. We identified a 2,4-dienoyl-CoA  
469 reductase (ORF 30) that may facilitate the next oxidation step to produce a NADH  
470 cofactor. FADH<sub>2</sub> and NADH molecules produced by a  $\beta$ -oxidation cycle can both be  
471 oxidized in the electron transport chain to generate ATP. The enzymes involved in the  
472 two intermediate steps following each oxidation, either an enoyl-CoA hydratase or a  
473  $\beta$ -ketothiolase, were not detected in our analysis.

474 Most of these genes have no homologs in reference viral genomes, and, to our  
475 knowledge, this is the first report of a virus possessing proteins directly involved in  
476 lipid-based energy production. By diverting host lipid machinery, interactions of  
477 viruses with lipids or lipid based-structures have long been known to have structural  
478 or signaling roles at different stages of the virus life cycle, such as entry, genome  
479 replication, morphogenesis, and exit (64–66). More recently, several studies on  
480 human viruses (two herpesviruses and one RNA virus) have shown that the metabolic  
481 state of an infected cell can be shifted toward energy generation to support viral  
482 replication (65). These studies have highlighted the increasing abundance—up to 48 h  
483 after HCV infection—of enzymes involved in  $\beta$ -oxidation, amino acid catabolism,  
484 and the TCA cycle (67) and an increase in cellular  $\beta$ -oxidation following the release  
485 of free fatty acids caused by Dengue virus-induced autophagy (68). Among algal  
486 viruses, EhV remodels the transcription of host lipid genes for fatty acid synthesis to  
487 support viral assembly (69) and also to generate triacylglycerols stored in the virion  
488 and available as an energy pool in later infection phases (70). Besides diverting the  
489 host metabolism, EhV encodes seven proteins involved in the sphingolipid  
490 biosynthesis pathway (71). This pathway produces a viral sphingolipid that is a  
491 central component of EhV lipid membranes and that can also act as a signaling lipid  
492 and induce programmed cell death during the lytic infection phase (72). EhV also  
493 encodes a triglyceride lipase (with detectable homology to predicted PkV RF01  
494 lipases ORF 635 and ORF653) that is highly expressed during late infection  
495 concomitantly with significant up-regulation of host  $\beta$ -oxidation genes (69). These  
496 examples and our observations of several genes involved in  $\beta$ -oxidation clearly show  
497 that viruses can introduce new metabolism-related genes, sometimes representing



498 entire pathways, into the host, most likely to satisfy the high metabolic requirement of  
499 these giant viruses.

### 500 **High representation of glycosyltransferases**

501 Compared with other viruses, PkV RF01 was found to encode an unusually high  
502 number of glycosyltransferases (GTs) as well as other carbohydrate-active enzymes  
503 ([Appendix – Results](#)). Automated annotation of GTs (and other carbohydrate-active  
504 enzymes) in reference viral proteomes using dbCAN2 (73) revealed that the largest  
505 number of GT domains was encoded by PkV RF01 ( $n = 48$ ), followed by CeV ( $n =$   
506 13), *Mimivirus* members, and CroV and AaV ( $n = 8–10$ ) ([Appendix – Fig. S8](#)). We  
507 uncovered 48 GT domains encoded in 40 ORFs, 8 of which were predicted to encode  
508 more than one GT domain. These domains correspond to 16 different GT families.  
509 Most domains were inferred to be functional, as 31 out of 48 covered at least 70% of  
510 the dbCAN2 reference domain, with coverage ranging from 44% to 99%. GTs were  
511 found scattered across the genome of PkV RF01 but with some local clustering ([Fig.](#)  
512 [2A](#)), the latter indicating possible involvement in the same pathway. GT32 was the  
513 most represented domain, with 11 proteins (as annotated by dbCAN2) and potentially  
514 three additional proteins (ORFs 40, 84, and 861). Eight proteins possessed a GT25  
515 domain that can catalyze the transfer of various sugars onto a growing  
516 lipopolysaccharide chain during its biosynthesis. Among these eight predicted ORFs,  
517 four contained an additional non-overlapping GT domain (two GT2s, one GT6, and  
518 one GT60). Functional analyses of GTs in mimiviruses (or in related *Paramecium*  
519 *bursaria* Chlorella viruses) have demonstrated that some of these enzymes are  
520 functional, being able to modify viral collagen-like proteins (74) and polymerize  
521 sugars (75). Conservation between PkV RF01 GTs and functionally characterized  
522 GTs in viruses and cells is absent or extremely low, which precludes any predictions



523 as to the specific roles of these enzymes in the PkV RF01 life cycle. Nevertheless, this  
524 putative glycosylation-conducive autonomy possibly allows the virus to infect a  
525 variety of hosts, as the virus can modify its own glycans, which are used for host  
526 recognition, independently of the host system (76). In alpha-, flavi-, and herpes-  
527 viruses, fusion is mediated by viral glycoproteins (40).

## 528 **Conclusions**

529 The haptophyte virus PkV RF01 has been previously shown to have a longer  
530 replication cycle and a broader host range compared with other prymnesioviruses and  
531 most other algal viruses. Here, we revealed that PkV RF01 has atypical virion  
532 morphology and that infections yield several orders of magnitude fewer infectious  
533 particles than other tested prymnesioviruses. In-depth phylogenetic analysis using  
534 genes conserved in NCLDV s confirmed that PkV RF01 belongs to *Mimiviridae* but is  
535 deeply diverged from existing members, although closer to alga-infecting  
536 *Mimiviridae* than heterotroph-infecting ones. Unlike other alga-infecting *Mimiviridae*,  
537 however, PkV RF01 has a large genome (1.4 Mb) and contains genes coding for two  
538 aminoacyl-tRNA synthetases and the complete BER pathway. All these features are  
539 conserved in most heterotroph-infecting *Mimiviridae* and therefore must have been  
540 lost in other alga-infecting *Mimiviridae*. This outlier virus features an  
541 unprecedentedly high number of genes involved in energy metabolism and  
542 glycosylation machinery that may enable its longer replication cycle and broader host  
543 range compared with other algal viruses. These genomic and phenotypic features are  
544 suggestive of a persistent infection behavior that probably evolved in response to the  
545 host growth strategy. Because of nutrient limitations, these persistent systems of slow-

546 growing but ubiquitous hosts with less virulent viruses may represent the most  
547 common type of virocells in oceans.

## 548 **Materials and Methods**

### 549 **PkV RF01 culturing and characterization**

550 Detailed materials and methods are provided in [Appendix – Materials and Methods](#).  
551 The details include information on culturing and infection, virus infectivity,  
552 sensitivity to chloroform, cryo-electron tomography, purification of viral particles and  
553 DNA isolation, and amplification and RT-PCR of *vSDHA*.

554 In brief, exponentially growing cultures of He UiO028 were infected with  
555 PkV RF01 at a virus-to-alga ratio of 10 to facilitate a one-step virus growth cycle  
556 (33). Infection was followed by flow cytometry counting (77, 78) to measure total  
557 VLPs and host cells. Furthermore, virus infectivity was determined by MPN (79)  
558 using He UiO028 as host and compared with that of two other prymnesioviruses,  
559 HeV RF02 and PkV RF02 (33), propagated on He UiO028 and *Prymnesium kappa*  
560 RCC3423, respectively. Sensitivity to chloroform, which suggests the presence of a  
561 lipid membrane or lipid molecules in the capsid, was tested in triplicate samples of  
562 exponentially growing HeUiO028 cells infected with a 1:10 volume of chloroform-  
563 treated PkV RF01 virus.

564 The structure of PkV RF01 was determined by cryo-electron tomography  
565 using a 200-kV transmission electron microscope (Talos F200C, Thermo Scientific)  
566 equipped with a Ceta 16M camera. Tilt series were recorded at 45,000× magnification  
567 and –7-μm defocus between –60° to 60° by 2° increments. Finally, reconstruction,  
568 segmentation, and visualization of tomograms was performed with the software  
569 package IMOD v4.9 (80).

570 Transcription of *vSDHA* was determined in an infected He UiO028 and PkV  
571 RF01 culture using an uninfected He UiO028 culture as a control. Samples were  
572 collected at 24, 72, and 96 h post infection from both cultures. RNA was extracted  
573 using the RNeasy Plus Universal Mini kit (Qiagen), with gDNA removed in an extra  
574 step using a TURBO DNA-free kit (Ambion). RT-PCRs were performed on the  
575 isolated mRNA using a SuperScript III One-Step RT-PCR with Platinum *Taq* DNA  
576 Polymerase system (Thermo Fisher).

577 DNA for PkV RF01 genome sequencing was isolated from 2 L of lysed He  
578 UiO028 culture. Algal debris and bacteria were removed by low-speed centrifugation.  
579 Viral particles were concentrated by ultracentrifugation at 25,000 rpm in a Beckman  
580 Coulter Optima L90K ultracentrifuge for 2 h and further purified by Optiprep gradient  
581 centrifugation (81). Isolation of high-quality DNA for sequencing was performed  
582 using the protocol described in (82) with some modifications. Total DNA was  
583 purified using a Zymo Genomic DNA Clean & Concentrator Kit-10 (Zymo Research,  
584 Irvine, CA, USA).

### 585 **Genome sequencing, assembly, and annotation**

586 DNA isolated from PkV RF01 was subjected to Illumina TruSeq PCR-free library  
587 preparation (insert size: 350 bp) and sequenced on an Illumina MiSeq instrument in  
588 paired-end mode ( $2 \times 300$  bp), thereby yielding approximately 1.9 million reads. In  
589 addition, a ligation-based 1D<sup>2</sup> nanopore library (LSK-308) was constructed and  
590 sequenced using an Oxford Nanopore MinION Mk1b device and a FLO-MIN107 flow  
591 cell, which resulted in 825 long reads with an N50 of 13.6 kbp comprising 9.89 Mbp in  
592 total. These data were assembled in a two-step process using Newbler (83) and Consed  
593 (84), and the consensus sequence was polished using Nanopolish (85) and Pilon (86).  
594 Genes were predicted using GeneMarkS (87) and tRNAscan-SE (88). Predicted protein

595 sequences were searched against various public databases using BLASTP, and  
596 significant alignments served as the basis for manual investigation on the GenomeNet  
597 (<https://www.genome.jp>) server to assign putative functions. [Appendix – Materials and](#)  
598 [Methods](#) contains further details on the genome assembly and annotation as well as  
599 specific methods used for reconstruction of each phylogenetic tree.

## 600 [Data availability](#)

601 Raw sequence reads and PkV RF01 genome sequence were deposited at the European  
602 Bioinformatics Institute (EMBL-EBI) (<https://www.ebi.ac.uk>) under project name  
603 PRJEB37450. The complete video records of a cryo-electron tomogram of a PkV  
604 RF01 virion and sequence data as well as curated gene annotation table as reported in  
605 this study are available at <https://github.com/RomainBlancMathieu/PkV-RF01>.

## 606 [Acknowledgements](#)

607 The recording of tilt series was performed with the help of Sebastian Schultz at the  
608 Unit of Cellular Electron Microscopy, the Norwegian Radium Hospital. Initial  
609 sequencing (MiSeq and Pacbio) of PkV RF01 total DNA was performed at the  
610 Norwegian Sequencing Center (<https://www.sequencing.uio.no/>). We thank Hilde M.  
611 K. Stabell and Solveig Siqveland, Department of Biological Sciences, University of  
612 Bergen, Norway, for technical assistance with molecular biology experiments as well  
613 as Christian Rückert, Bielefeld University, for support in manual finishing of genome  
614 assembly and Minyue Fan, Kyoto University, for assistance in genes analysis. This  
615 work was supported by the Research Council of Norway project entitled “Uncovering  
616 the key players for regulation of phytoplankton function and structure: lesson to be  
617 learned from algal virus-haptophyte coexistence” (VirVar, project number 294364 to  
618 RAS). Additional funding was provided by the European Union Horizons 2020  
619 research and innovation program, grant agreement no. 685778 (“Virus-X”) to RAS  
620 and DB. This work was also supported by the Future Development Funding Program  
621 of the Kyoto University Research Coordination Alliance. HO was supported by  
622 JSPS/KAKENHI (No. 18H02279), and Scientific Research on Innovative Areas from  
623 the Ministry of Education, Culture, Science, Sports and Technology (MEXT) of Japan  
624 (Nos. 16H06429, 16K21723, 16H06437). The Super Computer System, Institute for  
625 Chemical Research, Kyoto University, provided computational time. We thank  
626 Barbara Goodson, from Edanz Group ([www.edanzediting.com/ac](http://www.edanzediting.com/ac)), for editing the  
627 English text of a draft of this manuscript.

## 628 [Competing interests](#)

629 Authors declare having no competing interests.

## 630 **References**

- 631 1. Dupré JO. 2009. Varieties of Living Things: Life at the Intersection of Lineage  
632 and Metabolism. *Philosophy & Theory in Biology* 1.
- 633 2. Forterre P. 2012. Virocell Concept, The, p. a0023264. *In* John Wiley & Sons,  
634 Ltd (ed.), eLS. John Wiley & Sons, Ltd, Chichester, UK.
- 635 3. Raoult D, Forterre P. 2008. Redefining viruses: lessons from Mimivirus. *Nat*  
636 *Rev Microbiol* 6:315–319.
- 637 4. Claverie J-M. 2006. Viruses take center stage in cellular evolution. *Genome*  
638 *Biology* 7:110.
- 639 5. Mann NH, Cook A, Millard A, Bailey S, Clokie M. 2003. Bacterial  
640 photosynthesis genes in a virus. *Nature* 424:741–741.
- 641 6. Lindell D, Sullivan MB, Johnson ZI, Tolonen AC, Rohwer F, Chisholm SW.  
642 2004. Transfer of photosynthesis genes to and from Prochlorococcus viruses.  
643 *PNAS* 101:11013–11018.
- 644 7. Hurwitz BL, Hallam SJ, Sullivan MB. 2013. Metabolic reprogramming by  
645 viruses in the sunlit and dark ocean. *Genome Biol* 14:R123.
- 646 8. Thompson LR, Zeng Q, Kelly L, Huang KH, Singer AU, Stubbe J, Chisholm  
647 SW. 2011. Phage auxiliary metabolic genes and the redirection of cyanobacterial  
648 host carbon metabolism. *Proc Natl Acad Sci USA* 108:E757-764.
- 649 9. Anantharaman K, Duhaimé MB, Breier JA, Wendt KA, Toner BM, Dick GJ.  
650 2014. Sulfur Oxidation Genes in Diverse Deep-Sea Viruses. *Science* 344:757–  
651 760.
- 652 10. Lindell D, Jaffe JD, Johnson ZI, Church GM, Chisholm SW. 2005.  
653 Photosynthesis genes in marine viruses yield proteins during host infection.  
654 *Nature* 438:86–89.
- 655 11. Fridman S, Flores-Uribe J, Larom S, Alalouf O, Liran O, Yacoby I, Salama F,  
656 Bailleul B, Rappaport F, Ziv T, Sharon I, Cornejo-Castillo FM, Philosof A,  
657 Dupont CL, Sánchez P, Acinas SG, Rohwer FL, Lindell D, Béjà O. 2017. A  
658 myovirus encoding both photosystem I and II proteins enhances cyclic electron  
659 flow in infected Prochlorococcus cells. *Nat Microbiol* 2:1350–1357.
- 660 12. Raoult D, Audic S, Robert C, Abergel C, Renesto P, Ogata H, La Scola B, Suzan  
661 M, Claverie J-M. 2004. The 1.2-megabase genome sequence of Mimivirus.  
662 *Science* 306:1344–1350.
- 663 13. Schulz F, Yutin N, Ivanova NN, Ortega DR, Lee TK, Vierheilig J, Daims H,  
664 Horn M, Wagner M, Jensen GJ, Kyrpides NC, Koonin EV, Woyke T. 2017.  
665 Giant viruses with an expanded complement of translation system components.  
666 *Science* 356:82–85.

- 667 14. Abrahão J, Silva L, Silva LS, Khalil JYB, Rodrigues R, Arantes T, Assis F,  
668 Boratto P, Andrade M, Kroon EG, Ribeiro B, Bergier I, Seligmann H, Ghigo E,  
669 Colson P, Levasseur A, Kroemer G, Raoult D, Scola BL. 2018. Tailed giant  
670 Tupanvirus possesses the most complete translational apparatus of the known  
671 virosphere. *Nat Commun* 9:1–12.
- 672 15. Miller ES, Heidelberg JF, Eisen JA, Nelson WC, Durkin AS, Ciecko A,  
673 Feldblyum TV, White O, Paulsen IT, Nierman WC, Lee J, Szczypinski B, Fraser  
674 CM. 2003. Complete Genome Sequence of the Broad-Host-Range Vibriophage  
675 KVP40: Comparative Genomics of a T4-Related Bacteriophage. *J Bacteriol*  
676 185:5220–5233.
- 677 16. Yoshikawa G, Askora A, Blanc-Mathieu R, Kawasaki T, Li Y, Nakano M,  
678 Ogata H, Yamada T. 2018. *Xanthomonas citri* jumbo phage XacN1 exhibits a  
679 wide host range and high complement of tRNA genes. *Sci Rep* 8:4486.
- 680 17. Mizuno CM, Guyomar C, Roux S, Lavigne R, Rodriguez-Valera F, Sullivan  
681 MB, Gillet R, Forterre P, Krupovic M. 2019. Numerous cultivated and  
682 uncultivated viruses encode ribosomal proteins. *Nature Communications* 10:752.
- 683 18. Schvarcz CR, Steward GF. 2018. A giant virus infecting green algae encodes  
684 key fermentation genes. *Virology* 518:423–433.
- 685 19. Piacente F, Gaglianone M, Laugier ME, Tonetti MG. 2015. The Autonomous  
686 Glycosylation of Large DNA Viruses. *International Journal of Molecular*  
687 *Sciences* 16:29315–29328.
- 688 20. Schulz F, Roux S, Paez-Espino D, Jungbluth S, Walsh D, Denev VJ, McMahon  
689 KD, Konstantinidis KT, Eloie-Fadrosch EA, Kyrpides N, Woyke T. 2020. Giant  
690 virus diversity and host interactions through global metagenomics. *Nature* 1–7.
- 691 21. Needham DM, Yoshizawa S, Hosaka T, Poirier C, Choi CJ, Hehenberger E,  
692 Irwin NAT, Wilken S, Yung C-M, Bachy C, Kurihara R, Nakajima Y, Kojima  
693 K, Kimura-Someya T, Leonard G, Malmstrom RR, Mende DR, Olson DK, Sudo  
694 Y, Sudek S, Richards TA, DeLong EF, Keeling PJ, Santoro AE, Shirouzu M,  
695 Iwasaki W, Worden AZ. 2019. A distinct lineage of giant viruses brings a  
696 rhodopsin photosystem to unicellular marine predators. *PNAS* 116:20574–  
697 20583.
- 698 22. Roux S, Brum JR, Dutilh BE, Sunagawa S, Duhaimbe MB, Loy A, Poulos BT,  
699 Solonenko N, Lara E, Poulain J, Pesant S, Kandels-Lewis S, Dimier C, Picheral  
700 M, Searson S, Cruaud C, Alberti A, Duarte CM, Gasol JM, Vaqué D, Bork P,  
701 Acinas SG, Wincker P, Sullivan MB. 2016. Ecogenomics and potential  
702 biogeochemical impacts of globally abundant ocean viruses. *Nature* 537:689–  
703 693.
- 704 23. Nishimura Y, Watai H, Honda T, Mihara T, Omae K, Roux S, Blanc-Mathieu R,  
705 Yamamoto K, Hingamp P, Sako Y, Sullivan MB, Goto S, Ogata H, Yoshida T.  
706 2017. Environmental Viral Genomes Shed New Light on Virus-Host  
707 Interactions in the Ocean. *mSphere* 2.



- 708 24. Forterre P. 2013. The virocell concept and environmental microbiology. *ISME J*  
709 7:233–236.
- 710 25. Rosenwasser S, Ziv C, Creveld SG van, Vardi A. 2016. Virocell Metabolism:  
711 Metabolic Innovations During Host–Virus Interactions in the Ocean. *Trends in*  
712 *Microbiology* 24:821–832.
- 713 26. Coy SR, Gann ER, Pound HL, Short SM, Wilhelm SW. 2018. Viruses of  
714 Eukaryotic Algae: Diversity, Methods for Detection, and Future Directions.  
715 *Viruses* 10:487.
- 716 27. Gallot-Lavallée L, Blanc G, Claverie J-M. 2017. Comparative Genomics of  
717 *Chrysochromulina ericina* Virus and Other Microalga-Infecting Large DNA  
718 Viruses Highlights Their Intricate Evolutionary Relationship with the  
719 Established Mimiviridae Family. *Journal of Virology* 91:e00230-17.
- 720 28. Jacobsen A, Bratbak G, Heldal M. 1996. Isolation and characterization of a virus  
721 infecting *phaeocystis pouchetii* (prymnesiophyceae)1. *Journal of Phycology*  
722 32:923–927.
- 723 29. Baudoux A-C, Brussaard CPD. 2005. Characterization of different viruses  
724 infecting the marine harmful algal bloom species *Phaeocystis globosa*. *Virology*  
725 341:80–90.
- 726 30. Wagstaff BA, Vladu IC, Barclay JE, Schroeder DC, Malin G, Field RA. 2017.  
727 Isolation and Characterization of a Double Stranded DNA Megavirus Infecting  
728 the Toxin-Producing Haptophyte *Prymnesium parvum*. *Viruses* 9.
- 729 31. Egge ES, Johannessen TV, Andersen T, Eikrem W, Bittner L, Larsen A, Sandaa  
730 R-A, Edvardsen B. 2015. Seasonal diversity and dynamics of haptophytes in the  
731 Skagerrak, Norway, explored by high-throughput sequencing. *Mol Ecol*  
732 24:3026–3042.
- 733 32. Sandaa RA, Heldal M, Castberg T, Thyraug R, Bratbak G. 2001. Isolation and  
734 characterization of two viruses with large genome size infecting  
735 *Chrysochromulina ericina* (Prymnesiophyceae) and *Pyramimonas orientalis*  
736 (Prasinophyceae). *Virology* 290:272–280.
- 737 33. Johannessen TV, Bratbak G, Larsen A, Ogata H, Egge ES, Edvardsen B, Eikrem  
738 W, Sandaa R-A. 2015. Characterisation of three novel giant viruses reveals huge  
739 diversity among viruses infecting Prymnesiales (Haptophyta). *Virology*  
740 476:180–188.
- 741 34. Feldman HA, Wang SS. 1961. Sensitivity of Various Viruses to Chloroform.  
742 *Proceedings of the Society for Experimental Biology and Medicine* 106:736–  
743 738.
- 744 35. Martínez M, Boere A, Gilg I, van Lent J, Witte H, van Bleijswijk J, Brussaard C.  
745 2015. New lipid envelope-containing dsDNA virus isolates infecting  
746 *Micromonas pusilla* reveal a separate phylogenetic group. *Aquatic Microbial*  
747 *Ecology* 74:17–28.

- 748 36. Mirza SF, Staniewski MA, Short CM, Long AM, Chaban YV, Short SM. 2015.  
749 Isolation and characterization of a virus infecting the freshwater algae  
750 *Chrysochromulina parva*. *Virology* 486:105–115.
- 751 37. Mackinder LCM, Worthy CA, Biggi G, Hall M, Ryan KP, Varsani A, Harper  
752 GM, Wilson WH, Brownlee C, Schroeder DC. 2009. A unicellular algal virus,  
753 *Emiliana huxleyi* virus 86, exploits an animal-like infection strategy. *Journal of*  
754 *General Virology*, 90:2306–2316.
- 755 38. Huiskonen JT, Kivelä HM, Bamford DH, Butcher SJ. 2004. The PM2 virion has  
756 a novel organization with an internal membrane and pentameric receptor binding  
757 spikes. *Nat Struct Mol Biol* 11:850–856.
- 758 39. Yan X, Chipman PR, Castberg T, Bratbak G, Baker TS. 2005. The Marine Algal  
759 Virus PpV01 Has an Icosahedral Capsid with T=219 Quasisymmetry. *J Virol*  
760 79:9236–9243.
- 761 40. Huiskonen JT, Butcher SJ. 2007. Membrane-containing viruses with  
762 icosahedrally symmetric capsids. *Curr Opin Struct Biol* 17:229–236.
- 763 41. King AM, Lefkowitz E, Adams MJ, Carstens EB. 2011. *Virus Taxonomy: Ninth*  
764 *Report of the International Committee on Taxonomy of Viruses*. Elsevier.
- 765 42. Peralta B, Gil-Carton D, Castaño-Díez D, Bertin A, Boulogne C, Oksanen HM,  
766 Bamford DH, Abrescia NGA. 2013. Mechanism of Membranous Tunnelling  
767 Nanotube Formation in Viral Genome Delivery. *PLOS Biology* 11:e1001667.
- 768 43. Philippe C, Krupovic M, Jaomanjaka F, Claisse O, Petrel M, le Marrec C. 2018.  
769 Bacteriophage GC1, a Novel Tectivirus Infecting *Gluconobacter Cerinus*, an  
770 Acetic Acid Bacterium Associated with Wine-Making. *Viruses* 10.
- 771 44. Yan X, Yu Z, Zhang P, Battisti AJ, Chipman PR, Bajaj C, Bergoin M,  
772 Rossmann MG, Baker TS. 2009. The Capsid Proteins of a Large, Icosahedral  
773 dsDNA Virus. *J Mol Biol* 385:1287–1299.
- 774 45. Klose T, Rossmann MG. 2014. Structure of large dsDNA viruses. *Biol Chem*  
775 395:711–719.
- 776 46. Gowing MM. 1993. Large virus-like particles from vacuoles of phaeodarian  
777 radiolarians and from other marine samples. *Marine Ecology Progress Series*  
778 101:33–43.
- 779 47. Gromov BV, Mamkaeva KA. 1981. A virus infection in the synchronized  
780 population of the *Chlorococcum minutum* zoospores. *Algological Studies/Archiv*  
781 *für Hydrobiologie, Supplement Volumes* 252–259.
- 782 48. Bratbak G, Jacobsen A, Heldal M, Nagasaki K, Thingstad F. 1998. Virus  
783 production in *Phaeocystis pouchetii* and its relation to host cell growth and  
784 nutrition. *Aquatic Microbial Ecology* 16:1–9.
- 785 49. Zimmerman AE, Bachy C, Ma X, Roux S, Jang HB, Sullivan MB, Waldbauer  
786 JR, Worden AZ. 2019. Closely related viruses of the marine picoeukaryotic alga



- 787            *Ostreococcus lucimarinus* exhibit different ecological strategies. *Environ*  
788            *Microbiol* 21:2148–2170.
- 789    50.    Thomsen HA, Buck KR, Chavez FP. 1994. Haptophytes as components of  
790            marine phytoplankton. *DTU Research Database* 187–208.
- 791    51.    Berngruber TW, Froissart R, Choisy M, Gandon S. 2013. Evolution of Virulence  
792            in Emerging Epidemics. *PLOS Pathogens* 9:e1003209.
- 793    52.    Day T, Proulx SR. 2004. A General Theory for the Evolutionary Dynamics of  
794            Virulence. *The American Naturalist* 163:E40–E63.
- 795    53.    King AA, Shrestha S, Harvill ET, Bjørnstad ON. 2009. Evolution of Acute  
796            Infections and the Invasion-Persistence Trade-Off. *The American Naturalist*  
797            173:446–455.
- 798    54.    Brussaard CPD, Bratbak G, Baudoux A-C, Ruardij P. 2007. Phaeocystis and its  
799            interaction with viruses. *Biogeochemistry* 83:201–215.
- 800    55.    Leggett HC, Buckling A, Long GH, Boots M. 2013. Generalism and the  
801            evolution of parasite virulence. *Trends Ecol Evol (Amst)* 28:592–596.
- 802    56.    Woolhouse MEJ, Taylor LH, Haydon DT. 2001. Population Biology of  
803            Multihost Pathogens. *Science* 292:1109–1112.
- 804    57.    Johannessen TV, Larsen A, Bratbak G, Pagarete A, Edvardsen B, Egge ED,  
805            Sandaa R-A. 2017. Seasonal Dynamics of Haptophytes and dsDNA Algal  
806            Viruses Suggest Complex Virus-Host Relationship. *Viruses* 9.
- 807    58.    Gran-Stadniczeńko S, Krabberød AK, Sandaa R-A, Yau S, Egge E, Edvardsen  
808            B. 2019. Seasonal Dynamics of Algae-Infecting Viruses and Their Inferred  
809            Interactions with Protists. *Viruses* 11:1043.
- 810    59.    Fischer MG, Allen MJ, Wilson WH, Suttle CA. 2010. Giant virus with a  
811            remarkable complement of genes infects marine zooplankton. *Proc Natl Acad*  
812            *Sci USA* 107:19508–19513.
- 813    60.    Sandaa R-A, Dahle H, Brussaard CPD, Ogata H, Blanc-Mathieu R. Algal  
814            viruses belonging to a subgroup within the Mimiviridae family *Encyclopedia of*  
815            *Virology*, 4th ed. Bamford, D., M. Zuckerman, Elsevier, Academic.
- 816    61.    Tatusov RL, Galperin MY, Natale DA, Koonin EV. 2000. The COG database: a  
817            tool for genome-scale analysis of protein functions and evolution. *Nucleic Acids*  
818            *Res* 28:33–36.
- 819    62.    Blanc-Mathieu R, Ogata H. 2016. DNA repair genes in the Megavirales  
820            pangenome. *Current Opinion in Microbiology* 31:94–100.
- 821    63.    Moniruzzaman M, Martinez-Gutierrez CA, Weinheimer AR, Aylward FO. 2020.  
822            Dynamic genome evolution and complex virocell metabolism of globally-  
823            distributed giant viruses. 1. *Nature Communications* 11:1710.

- 824 64. Ono A. 2010. Viruses and Lipids. *Viruses* 2:1236–1238.
- 825 65. Heaton NS, Randall G. 2011. Multifaceted roles for lipids in viral infection.  
826 *Trends Microbiol* 19:368–375.
- 827 66. Lange PT, Lagunoff M, Tarakanova VL. 2019. Chewing the Fat: The Conserved  
828 Ability of DNA Viruses to Hijack Cellular Lipid Metabolism. *Viruses* 11:119.
- 829 67. Diamond DL, Syder AJ, Jacobs JM, Sorensen CM, Walters K-A, Proll SC,  
830 McDermott JE, Gritsenko MA, Zhang Q, Zhao R, Metz TO, Camp DG, Waters  
831 KM, Smith RD, Rice CM, Katze MG. 2010. Temporal Proteome and Lipidome  
832 Profiles Reveal Hepatitis C Virus-Associated Reprogramming of Hepatocellular  
833 Metabolism and Bioenergetics. *PLoS Pathog* 6.
- 834 68. Heaton NS, Randall G. 2010. Dengue virus induced autophagy regulates lipid  
835 metabolism. *Cell Host Microbe* 8:422–432.
- 836 69. Rosenwasser S, Mausz MA, Schatz D, Sheyn U, Malitsky S, Aharoni A,  
837 Weinstock E, Tzfadia O, Ben-Dor S, Feldmesser E, Pohnert G, Vardi A. 2014.  
838 Rewiring Host Lipid Metabolism by Large Viruses Determines the Fate of  
839 *Emiliana huxleyi*, a Bloom-Forming Alga in the Ocean[C][W][OPEN]. *Plant*  
840 *Cell* 26:2689–2707.
- 841 70. Malitsky S, Ziv C, Rosenwasser S, Zheng S, Schatz D, Porat Z, Ben-Dor S,  
842 Aharoni A, Vardi A. 2016. Viral infection of the marine alga *Emiliana huxleyi*  
843 triggers lipidome remodeling and induces the production of highly saturated  
844 triacylglycerol. *New Phytologist* 210:88–96.
- 845 71. Wilson WH, Schroeder DC, Allen MJ, Holden MTG, Parkhill J, Barrell BG,  
846 Churcher C, Hamlin N, Mungall K, Norbertczak H, Quail MA, Price C,  
847 Rabinowitsch E, Walker D, Craigon M, Roy D, Ghazal P. 2005. Complete  
848 Genome Sequence and Lytic Phase Transcription Profile of a Coccolithovirus.  
849 *Science* 309:1090–1092.
- 850 72. Vardi A, Van Mooy BAS, Fredricks HF, Popenorf KJ, Ossolinski JE,  
851 Haramaty L, Bidle KD. 2009. Viral glycosphingolipids induce lytic infection  
852 and cell death in marine phytoplankton. *Science* 326:861–865.
- 853 73. Zhang H, Yohe T, Huang L, Entwistle S, Wu P, Yang Z, Busk PK, Xu Y, Yin Y.  
854 2018. dbCAN2: a meta server for automated carbohydrate-active enzyme  
855 annotation. *Nucleic Acids Res* 46:W95–W101.
- 856 74. Luther KB, Hülsmeier AJ, Schegg B, Deuber SA, Raoult D, Hennet T. 2011.  
857 Mimivirus collagen is modified by bifunctional lysyl hydroxylase and  
858 glycosyltransferase enzyme. *J Biol Chem* 286:43701–43709.
- 859 75. Rommel AJ, Hülsmeier AJ, Jurt S, Hennet T. 2016. Giant mimivirus R707  
860 encodes a glycogenin paralogue polymerizing glucose through  $\alpha$ - and  $\beta$ -  
861 glycosidic linkages. *Biochem J* 473:3451–3462.
- 862 76. Parakkottil Chothi M, Duncan GA, Armirotti A, Abergel C, Gurnon JR, Van  
863 Etten JL, Bernardi C, Damonte G, Tonetti M. 2010. Identification of an l-

- 864 Rhamnose Synthetic Pathway in Two Nucleocytoplasmic Large DNA Viruses. *J*  
865 *Virol* 84:8829–8838.
- 866 77. Marie D, Brussaard CPD, Thyraug R, Bratbak G, Vaultot D. 1999. Enumeration  
867 of Marine Viruses in Culture and Natural Samples by Flow Cytometry. *Appl*  
868 *Environ Microbiol* 65:45–52.
- 869 78. Brussaard CPD. 2004. Optimization of procedures for counting viruses by flow  
870 cytometry. *Appl Environ Microbiol* 70:1506–1513.
- 871 79. Suttle CA, Chan AM. 1993. Marine cyanophages infecting oceanic and coastal  
872 strains of *Synechococcus*: abundance, morphology, cross-infectivity and growth  
873 characteristics. *Marine ecology progress series*  
874 <https://doi.org/10.3354/meps092099>.
- 875 80. Kremer JR, Mastrorarde DN, McIntosh JR. 1996. Computer visualization of  
876 three-dimensional image data using IMOD. *J Struct Biol* 116:71–76.
- 877 81. Lawrence JE, Steward GF. 2010. Purification of viruses by centrifugation, p.  
878 166–181. *In* Wilhelm, S, Weinbauer, M, Suttle, C (eds.), *Manual of Aquatic*  
879 *Viral Ecology*. American Society of Limnology and Oceanography.
- 880 82. Sandaa R-A, E. Storesund J, Olesin E, Lund Paulsen M, Larsen A, Bratbak G,  
881 Ray JL. 2018. Seasonality Drives Microbial Community Structure, Shaping both  
882 Eukaryotic and Prokaryotic Host–Viral Relationships in an Arctic Marine  
883 Ecosystem. *Viruses* 10.
- 884 83. Margulies M, Egholm M, Altman WE, Attiya S, Bader JS, Bemben LA, Berka J,  
885 Braverman MS, Chen Y-J, Chen Z, Dewell SB, Du L, Fierro JM, Gomes XV,  
886 Godwin BC, He W, Helgesen S, Ho CH, Irzyk GP, Jando SC, Alenquer MLI,  
887 Jarvie TP, Jirage KB, Kim J-B, Knight JR, Lanza JR, Leamon JH, Lefkowitz  
888 SM, Lei M, Li J, Lohman KL, Lu H, Makhijani VB, McDade KE, McKenna  
889 MP, Myers EW, Nickerson E, Nobile JR, Plant R, Puc BP, Ronan MT, Roth GT,  
890 Sarkis GJ, Simons JF, Simpson JW, Srinivasan M, Tartaro KR, Tomasz A, Vogt  
891 KA, Volkmer GA, Wang SH, Wang Y, Weiner MP, Yu P, Begley RF, Rothberg  
892 JM. 2005. Genome sequencing in microfabricated high-density picolitre  
893 reactors. *Nature* 437:376–380.
- 894 84. Gordon D, Green P. 2013. Consed: a graphical editor for next-generation  
895 sequencing. *Bioinformatics* 29:2936–2937.
- 896 85. Loman NJ, Quick J, Simpson JT. 2015. A complete bacterial genome assembled  
897 de novo using only nanopore sequencing data. *Nat Methods* 12:733–735.
- 898 86. Walker BJ, Abeel T, Shea T, Priest M, Abouelliel A, Sakthikumar S, Cuomo  
899 CA, Zeng Q, Wortman J, Young SK, Earl AM. 2014. Pilon: An Integrated Tool  
900 for Comprehensive Microbial Variant Detection and Genome Assembly  
901 Improvement. *PLOS ONE* 9:e112963.
- 902 87. Besemer J, Lomsadze A, Borodovsky M. 2001. GeneMarkS: a self-training  
903 method for prediction of gene starts in microbial genomes. Implications for  
904 finding sequence motifs in regulatory regions. *Nucleic Acids Res* 29:2607–2618.

- 905 88. Lowe TM, Chan PP. 2016. tRNAscan-SE On-line: integrating search and  
906 context for analysis of transfer RNA genes. *Nucleic Acids Res* 44:W54-57.  
907

1	<b>Appendix</b>	
2		
3	Materials and Methods .....	2
4	Culturing and infection.....	2
5	Infectious progeny.....	2
6	Sensitivity to chloroform.....	2
7	Cryo-electron tomography .....	2
8	Purification of viral particles and DNA isolation.....	3
9	Genome assembly .....	3
10	Phylogenetic analyses .....	3
11	Five core genes, SDHA, and SDHB .....	3
12	Rpb2, IleRS, and AsnRS .....	4
13	Gene prediction and functional and taxonomic annotation.....	4
14	Taxonomic and functional analysis of vSDHA homologs in OM-RGCv1.....	5
15	PCR and RT-PCR optimization .....	5
16	PCR amplification and RT-PCR analysis of vSDHA .....	5
17	Results .....	6
18	DNA repair enzymes .....	6
19	Transcription .....	6
20	Translation.....	6
21	Other carbohydrate-active enzymes .....	7
22	Figures .....	8
23	Fig. S1. Reduction of PkV RF01 infectivity with chloroform. ....	8
24	Fig. S2. High density of exact small repeats in the PkV RF01 genome. ....	9
25	Fig. S3. COG functional distribution of 339 proteins encoded by PkV RF01.....	10
26	Fig. S4. Comparative COG functional distribution among <i>Mimiviridae</i> members. ....	11
27	Fig. S5. Bayesian phylogenetic trees of two viral amino-acyl tRNA synthetases and their	
28	cellular homologs. ....	12
29	Fig. S6. PCR optimization and confirmation of the <i>SDHA</i> gene in the PkV RF01 genome.	
30	.....	13
31	Fig. S7. PCR and RT-PCR optimization using an internal control gene ( <i>mcp</i> ). ....	14
32	Fig. S8. Comparative distribution of glycosyltransferase domains among viruses. ....	15
33	Tables .....	16
34	Table S1. Type and position of 40 predicted tRNA genes in the PkV RF01 genome .....	16
35	Table S2. Genes related to lipid metabolism.....	17
36	Table S3. Details for tree reconstruction.....	17
37	Table S4. Forward and reverse PCR primers for amplification of vSDHA and MCP .....	17
38	References .....	18
39		

## 40 **Materials and Methods**

### 41 **Culturing and infection**

42 All algal host cultures were grown in liquid IMR/2 medium consisting of 70% aged seawater,  
43 30% distilled water (25 PSU), and additional selenite (10 nM final concentration). The  
44 cultures were kept at 14°C and partially synchronized using a 14:10 h light: dark cycle with  
45 irradiance of 100  $\mu\text{mol photons m}^{-2} \text{ s}^{-2}$  supplied by white fluorescent tubes. Viruses were  
46 produced by adding freshly produced viral lysate (ca.  $2 \times 10^8$  VLP/mL), propagated three  
47 time on the host before added to exponentially growing host cultures (ca.  $5 \times 10^5$  cells/mL) in a  
48 ratio of 1:10 volume. Infection was followed by flow cytometry (FCM) (1, 2) for 72 h by  
49 counting viral particles and host cells, as described in (3). Burst size was calculated as the  
50 number of viral particles released from each host cell, estimated from the total number of host  
51 cells pre-infection and the total number of VLPs produced during the infection cycle (3).

### 52 **Infectious progeny**

53 The percentage of viral infectious progeny was determined by comparing the most probable  
54 number (MPN; endpoint dilution (2)) and flow cytometric total counts of viral particles  
55 produced during infection. The number of infectious particles released in a burst was  
56 determined based on the percentage of viral infectivity produced during the infection cycle  
57 and the burst size. Infectivity was tested using *Haptolina ericina* UiO028 as a host, and also  
58 compared with two other prymnesioviruses, HeV RF02 and PkV RF02 (3), propagated on He  
59 UiO028 and *Prymnesium kappa* RCC3423, respectively.

60  
61 Briefly, 10 $\times$  dilution were prepared from fresh viral lysate and added to exponentially  
62 growing host cells in 96-well microtiter plates (eight replicates for each dilution). The plates  
63 were incubated for 7 days under normal incubation conditions. Cell lysis was measured by  
64 monitoring *in situ* fluorescence on a plate reader (PerkinElmer EnSpire™ 2300 Multilabel  
65 Reader) at 460/680 nm. Numbers of infectious particles were estimated from the proportion of  
66 lysed wells using the MPN\_ver4.xls excel spreadsheet from (4).

### 67 **Sensitivity to chloroform**

68 The effect of chloroform on infectivity, used to infer the presence of a lipid membrane or lipid  
69 molecules in the capsid, was tested by adding 50% (v/v) chloroform to PkV RF01 lysate.  
70 After mixing, the chloroform phase was separated from the solution by centrifugation at 4,000  
71 g for 5 min. The tubes were incubated at 37°C for 2 h with the lids open to allow evaporation  
72 of any remaining chloroform.

73  
74 Triplicates of exponentially growing He UiO028 cells ( $1.6 \times 10^5$  cells /mL) were incubated  
75 with 1:10 volumes of chloroform-treated viruses (ca.  $2 \times 10^8$  VLP/mL). The incubation was  
76 followed for 7 days by counting host cells by FCM (2). Host cells in chloroform-treated or  
77 untreated medium at the same ratio used with the viral lysate were used as controls. Virus  
78 propagation was confirmed in lysed cultures by FCM.

### 79 **Cryo-electron tomography**

80 A small drop of concentrated PkV RF01 ( $8 \times 10^9$ ) was deposited on a glow-discharged, 200-  
81 mesh copper grid with holey carbon film (R2/1 Cu 200, Quantifoil Micro Tools GmbH,  
82 Germany). The sample was blotted with filter paper and immediately plunge frozen in liquid  
83 ethane. Grids were transferred under liquid nitrogen to a cryo-transfer tomography holder  
84 (Fishione Instruments, USA) and inserted in a 200-kV transmission electron microscope  
85 (Thermo Scientific Talos F200C) equipped with a Ceta 16M camera. Tilt series were recorded



86 at 45,000× magnification and  $-7\ \mu\text{m}$  defocus between  $-60^\circ$  to  $60^\circ$  in  $2^\circ$  increments. Finally,  
87 reconstruction, segmentation, and visualization of the tomograms was performed with IMOD  
88 v4.9 software (5).

### 89 **Purification of viral particles and DNA isolation**

90 Exponentially growing He UiO028 cultures (2 L) were infected with 20 mL of PkV RF01 and  
91 inspected visually for lysis. An uninfected culture (100 mL) was used as a control. Lysed  
92 algal cultures were checked for viruses by FCM counting. Lysed cultures were first  
93 centrifuged to remove algal debris and some bacteria (5,500 rpm for 15 min). Viruses were  
94 then pelleted by ultracentrifugation at 25,000 rpm in a Beckman Coulter Optima L90K  
95 ultracentrifuge for 2 h. The pellets were resuspended in SM buffer (0.1 M NaCl, 8 mM  
96  $\text{MgSO}_4 \cdot 7\text{H}_2\text{O}$ , 50 mM Tris-HCl, and 0.005% glycerin). Viral particles were further purified  
97 by Optiprep gradient centrifugation (6). Fractions were checked for viruses by FCM and for  
98 infectivity by infection of He UiO028.

99  
100 Isolation of high-quality DNA for sequencing was done by following the protocol of (7) with  
101 some modifications. Viral particles were disrupted by one round of heating to  $90^\circ\text{C}$  for 2 min  
102 and then chilling on ice for 2 min. Disodium ethylenediaminetetraacetic acid and proteinase K  
103 at a final concentration of 20 mM and  $100\ \mu\text{g mL}^{-1}$ , respectively, were then added before  
104 incubation of the samples for 10 min at  $55^\circ\text{C}$ . Sodium dodecyl sulfate at a final concentration  
105 of 0.5% (w/v) was subsequently added, and samples were incubated for an additional 1 h at  
106  $55^\circ\text{C}$ . Double-stranded DNA was then purified from the lysates using a Zymo Genomic DNA  
107 Clean & Concentrator Kit-10 (Zymo Research, Irvine, CA, USA) according to the  
108 manufacturer's protocols. To avoid shearing DNA, gentle pipetting and mixing (accomplished  
109 by turning the tubes instead of vortexing) were performed in all steps.

### 110 **Genome assembly**

111 Isolated DNA from PkV RF01 was subjected to Illumina TruSeq PCR-free library preparation  
112 (insert size 350 bp). The generated library was sequenced on an Illumina MiSeq instrument in  
113 paired-end mode ( $2 \times 300$  bp) to yield approximately 1.9 million reads, which corresponds to  
114 about  $400\times$  coverage. Reads were assembled into 2,498 contigs of 500 bp or more with a total  
115 assembly size of 4.75 Mb using Newbler (8). In addition, a ligation-based 1D<sup>2</sup> nanopore  
116 library (LSK-308) was constructed and sequenced using an Oxford Nanopore MinION Mk1b  
117 device and a FLO-MIN107 flow cell, which resulted in 825 long reads with an N50 of 13.6 kb  
118 and a total of 9.89 Mb. To improve the assembly, short-read contigs were manually bridged  
119 with the long reads. Manual assembly using Consed (9) yielded a linear genome sequence of  
120 1.4 Mb with inverted terminal repeats. After assembly, the consensus was polished using  
121 Nanopolish (10) and Pilon (11).

### 122 **Phylogenetic analyses**

#### 123 **Five core genes, SDHA, and SDHB**

124 The phylogenetic position of PkV RF01 was inferred from concatenated protein alignments of  
125 five core nucleocytoplasmic virus orthologous genes (NCVOGs) (12): D5-like helicase-  
126 primase (NCVOG0023), DNA polymerase elongation subunit family B (NCVOG0038), DNA  
127 or RNA helicases of superfamily II (NCVOG0076), packaging ATPase (NCVOG0249), and  
128 Poxvirus Late Transcription Factor VLTF3-like (NCVOG0262). Sequences were obtained  
129 from the NCVOG database (<ftp.ncbi.nlm.nih.gov/pub/wolf/COGs/NCVOG/>) (13). Additional  
130 sequences were obtained from genomes retrieved from GenBank and annotated with  
131 HMMER v3.12b using the hmmsearch (14) command with hidden Markov models available  
132 in Schults et al. (2017) (15). Sequences from each NCVOG were aligned independently using

133 MAFFT L-INS-i (16). The alignments were trimmed with trimAl v1.2 in *gappyout* mode (17)  
134 prior to concatenation using a custom Python script. Bayesian phylogenetic trees were  
135 inferred with PhyloBayes 1.7 (18) using the CAT model and a GTR substitution matrix. Four  
136 chains were run for 34,500–35,500 generations. The *bpcomp* command was used to check for  
137 convergence. One chain was discarded, and a consensus tree was constructed using the  
138 remaining three chains.

139  
140 For phylogenetic analyses of succinate dehydrogenase subunits, top hits of PkV RF01 SDHA  
141 and SDHB were retrieved from UniProt (<https://www.uniprot.org/>) using online PHMMR  
142 searches (<https://www.ebi.ac.uk/Tools/hmmer/search/phmmer>) and also from the *Tara*  
143 Oceans project using online BLASTP searches ([http://tara-oceans.mio.osupytheas.fr/ocean-](http://tara-oceans.mio.osupytheas.fr/ocean-gene-atlas/)  
144 [gene-atlas/](http://tara-oceans.mio.osupytheas.fr/ocean-gene-atlas/)) (Villar et al., 2018). Alignments generated with MAFFT L-INS-i were filtered  
145 with trimAl in *gappyout* mode. Maximum-likelihood phylogenies were inferred with RAxML  
146 8.2.9 (19) using the PROTCATALG model and automatic bootstrapping with the following  
147 options: ‘-N autoMRE -f a -n autoresult’. Phylogenetic trees of PkV RF01, SDHA, and SDHB  
148 were visualized using iTOL (20).

149  
150 **Rpb2, IleRS, and AsnRS**

151 To reconstruct a phylogenetic tree based on the second largest RNA polymerase subunit,  
152 homologs were recruited by comparing Mimivirus Rpb2 against all proteins of viruses and  
153 selected organisms in the KEGG database using the GenomeNet BLASTP tool  
154 (<https://www.genome.jp/>). Organisms were manually selected from the KEGG list to ensure  
155 broad taxonomic coverage of the tree of life. The retrieved amino acid sequences were  
156 aligned using MAFFT-LINSI (16) and then trimmed using trimAl (17) with the following  
157 parameters: ‘-resoverlap 0.5 -seqoverlap 70 -gt 0.8 -st 0.001 -cons 50’. The tree was  
158 reconstructed using FastTree (21) as implemented in the GenomeNet TREE tool  
159 (<https://www.genome.jp/tools-bin/ete>). Isoleucine tRNA synthase and aspartyl tRNA  
160 synthetase viral and cellular homologs were retrieved and aligned in the same way. Trees  
161 were searched using PhyloBayes MPI (22) with the non-homogeneous CAT+GTR model  
162 (23). Details of the PhyloBayes runs for each tree are provided in Table S3.

### 163 **Gene prediction and functional and taxonomic annotation**

164 GeneMarkS with the option ‘virus’ (24) predicted 1,121 open reading frames (ORFs) in the  
165 fully assembled genome sequence of PkV RF01, while tRNAscan-SE (25) predicted 41  
166 tRNAs. PkV RF01 CDS amino acid sequences were searched against Virus-Host DB (26),  
167 RefSeq (27), UniRef90 (28), and COG (29) databases using BLASTP with an *E*-value of  $1 \times$   
168  $10^{-5}$  as the significant similarity threshold and against the Conserved Domain Database (30)  
169 using RPS-BLAST with an *E*-value threshold of  $1 \times 10^{-2}$ . The 10 best hits for each database  
170 were compiled in a single file and manually inspected to transfer annotations of subject  
171 sequences to our query. In ambiguous cases, such as distant homologs (often seen in viral  
172 genomes) or unclear or contradictory annotations of subject sequences, the query was  
173 searched against KEGG genes (31) to allow extensive manual checking using GenomeNet  
174 tools (<https://www.genome.jp/>; alignment quality, length comparison to canonical genes, and  
175 links with KEGG orthology). We automatically annotated glycosyltransferases (GTs) and  
176 other carbohydrate-active enzymes (glycoside hydrolases, GHs; polysaccharide lyases, PLs;  
177 carbohydrate esterases, CEs; and auxiliary activities, AAs) in PkV RF01 and all viral  
178 genomes in Virus-Host DB (as of June 2018) using the *hmm* option of the dbCAN2 pipeline  
179 and its profile database (32). We retained hits with *E*-values  $< 1 \times 10^{-5}$  and domain coverage  
180  $> 35\%$ , which corresponded to default settings. Sequence-based identification of paralogous  
181 genes in the PkV RF01 proteome was conducted using OrthoFinder (33) with default



182 parameters. Transfer of functional information onto the largest group of paralogs, which  
183 contained six proteins (with all other groups containing only two), was conducted as follows:  
184 sequences were aligned using MAFFT-LINSI and searched against the “uniclust30” database  
185 using the HHPred toolkit (34) at <https://toolkit.tuebingen.mpg.de>. We considered hits with  
186 probabilities > 99%.  
187

### 188 **Taxonomic and functional analysis of vSDHA homologs in OM-RGCv1**

189 We searched PkV RF01 SDHA and SDHB against OM-RGCv1 (35) using the Ocean Gene  
190 Atlas (36) BLAST-based tool and kept the top 50 hits with significant *E*-values for further  
191 analysis. We then collected genome fragments (contigs) encoding these 50 SDHAs and 50  
192 SDHBs by searching via BLASTN for identical hits over full *SDHA* or *SDHB* lengths against  
193 *Tara* ocean assemblies (downloaded from EBI) used to construct OM-RGCv1 (35). We  
194 predicted ORFs in these genome fragments using GeneMarkS. The resulting 1,113 amino acid  
195 sequences were functionally annotated by searching against Pfam protein families (37) using  
196 profile HMM scan (38) and also taxonomically using a last common ancestor strategy as in  
197 (39); in brief, protein sequences were searched against a database composed of UniRef cells,  
198 MMETSP (40) and Virus-Host DB (26) data using DIAMOND (41). Selected hits were then  
199 used to derive the last common ancestor of the query using a NCBI taxonomic tree re-wired to  
200 reflect the taxonomy of NCLDV.

### 201 **PCR and RT-PCR optimization**

202 We designed specific primers (Table S4) targeting a 256-bp region of the *mcp* gene to use  
203 both as an internal control in the RT-PCR and to confirm that our protocols were optimized.  
204 For each PCR, a negative control (sterile distilled H<sub>2</sub>O) was included. PCR amplifications  
205 were carried out in 50- $\mu$ L total volumes containing 1  $\mu$ L of template using a DNA  
206 HotStarTaq Master Mix kit (Qiagen). The cycling protocol was as follows: 15 min at 95°C,  
207 followed by 35 cycles of 30 s at 94°C, 30 s at 59°C, and 30 s at 72°C, with a final extension  
208 of 12 min at 72°C.  
209

210 RT-PCRs were performed using the SuperScript III One-Step RT-PCR with Platinum *Taq*  
211 DNA Polymerase system (Thermo Fisher). Cycling conditions were as follows: 16 min at  
212 55°C and 2 min at 94°C, followed by 40 cycles of 15 s at 94°C, 30 s at 49°C, and 30 s at  
213 68°C, and a final extension of 5 min at 68°C.  
214

215 All PCR products were checked for the correct size on a 1.5% agarose gel stained with  
216 GelRed (Biotium). PCR products were further checked by sequencing using BigDye v3.1  
217 (Thermo Fisher) for cycle sequencing (Sekvenseringslaboratoriet, UiB, Norway).

### 218 **PCR amplification and RT-PCR analysis of vSDHA**

219 To investigate whether the *vSDHA* gene is transcribed during infection, an infected culture of  
220 He\_UiO028 plus PkV RF01 as well as an uninfected He\_UiO028 culture (control) were set up  
221 as described above. Samples were collected at 24, 72, and 96 h post infection from both  
222 cultures. RNA was extracted using an RNeasy Plus Universal Mini kit (Qiagen), with gDNA  
223 removed in an extra step using a TURBO DNA-free kit (Ambion).  
224

225 Specific primers were designed to target a 150-bp region of the *vSDHA* gene (Table S4). For  
226 each PCR, two negative controls (sterile distilled H<sub>2</sub>O and extracted DNA from He028) were  
227 included. As positive controls for the transcription, we used primers targeting the *mcp* gene  
228 (see above). As a positive PCR control, we used genomic PkV RF01 DNA. PCR  
229 amplifications were conducted in 50- $\mu$ L total volumes containing 1  $\mu$ L of template DNA

230 using an ExTaq kit (Takara). The cycling protocol was as follows: 5 min at 94°C, followed by  
231 35 cycles of 30 s at 94°C, 30 s at 59°C, and 30 s at 72°C, with a final extension of 12 min  
232 extension at 72°C.

233  
234 RT-PCRs were performed using a SuperScript III One-Step RT-PCR with Platinum Taq DNA  
235 Polymerase system (Thermo Fisher). Cycling conditions were as follows: 16 min at 55°C and  
236 2 min at 94°C, followed by 40 cycles of 15 s at 94°C, 30 s at 49°C, and 30 s at 68°C, with a  
237 final extension of 5 min at 68°C. PCR products were checked as described above.

## 238 **Results**

### 239 **DNA repair enzymes**

240 NCLDV members are known to encode several genes corresponding to major DNA repair  
241 pathways, with some members encompassing full, or nearly full, pathway representation, such  
242 as the base excision repair (BER) pathway of Mimivirus (42). While some of these genes  
243 were acquired relatively recently from cellular organisms, others are connected with the early  
244 evolutionary history of these viruses (43). PkV RF01 also encodes a set of enzymes needed to  
245 facilitate the BER pathway, namely, two DNA glycosylases (ORF 196 and ORF 871), an  
246 apurinic-apyrimidinic (AP) endonuclease (ORF 935), a family-X DNA polymerase (ORF  
247 630), and a NAD-dependent DNA ligase (ORF 741). These enzymes are conserved in all  
248 *Mimiviridae* members except for those with relatively small genomes (PgV, CeV, and AaV).  
249 In PgV and CeV, but not AaV and PkV RF01, the family-X DNA polymerase and DNA  
250 ligase are fused. The presence of these BER enzymes in PkV RF01 suggests that this viral  
251 BER pathway was already present in the last common ancestor of *Mimiviridae*. As in all other  
252 *Mimiviridae*, PkV RF01 encodes MutS7, a key enzyme of the mismatch repair pathway, and  
253 the MutS8 homolog—thus far only observed in PgV and CeV. Enzymes involved in other  
254 DNA repair pathways, such as XPG/Rad2 endonuclease (present in *Mimivirus* and CroV) and  
255 the fused Mre11-Rad50 DNA break repair protein (present in Mimivirus members only), were  
256 not found in PkV RF01.

### 257 **Transcription**

258 Similar to other *Mimiviridae*, PkV RF01 encodes several transcription-related genes,  
259 including those coding for several subunits of eukaryotic DNA-dependent RNA polymerase  
260 type II (RPB1, RPB2 [ $\times 2$ ], RPB3, RPB5, RPB6, RPB7, RPB9, and RPB10, the latter not  
261 present in other *Mimiviridae* besides BsV and HKV1); transcription initiation (ORF306),  
262 elongation (ORF856), late (ORF436), and termination (ORF275) factors; a TATA-box-like  
263 binding protein (ORF709); and a mRNA capping enzyme (ORF42)—but not the polyA  
264 polymerase seen in other *Mimiviridae*. PkV RF01 also encodes a cold-shock protein (ORF  
265 1082) shared with CeV and PgV that may prevent the formation of secondary structures in  
266 mRNA at low temperature and thus facilitate the initiation of translation (44).

### 267 **Translation**

268 A striking feature of *Mimiviridae* is the high prevalence of genes coding for translation-  
269 associated proteins. In particular, amino-acyl tRNA synthetases (aaRSs) are found in all  
270 heterotroph-infecting *Mimiviridae*—ranging from 1 in CroV to 20 in Tupanvirus—but are  
271 missing from alga-infecting *Mimiviridae*, although CeV encodes a catalytic domain for  
272 Asn/Asp-RNAt synthetase. Phylogenetic analyses of the two aaRSs encoded in PkV-RF01  
273 revealed a deep branching of viral homologs, which formed a monophyletic clade well  
274 separated from cellular homologs (Fig. S5). Although the phylogenetic relationship among  
275 viruses on these trees does not exactly reflect their classification (e.g., Orpheovirus within

276 Megavirinae), the recovered topologies suggest an ancient history for these genes rather than  
277 a recent acquisition from cellular organisms. The IleRS tree (Fig. S5A) is in agreement with  
278 previous phylogenetic analyses of cellular organisms with the known split of bacterial  
279 lineages (45, 46). In our tree, *Mimiviridae* and Orpheovirus form a monophyletic group  
280 branching at the root of eukaryotic organisms, which suggests that the IleRS gene was  
281 acquired before the divergence of extant eukaryotic phyla or from a now-extinct or as yet  
282 unknown eukaryotic phylum at the root of the eukaryotic tree. Similarly, the AsnRS tree  
283 supports the presence of this enzyme in the ancestor of *Mimiviridae* (Fig. S5B). Alternatively,  
284 rapid evolution of more recently acquired genes could generate these observed topologies in a  
285 phenomenon known as the long-branch attraction bias (47). Nonetheless the branches for  
286 viruses were not particularly long compared to the branches for eukaryotes and the  
287 evolutionary model used in our phylogenetic analyses is known to minimize this bias  
288 (compared to more traditional models) (48, 49). Therefore, it seems more likely that viral  
289 genes were recruited from proto-eukaryotes before the diversification of modern eukaryotes.

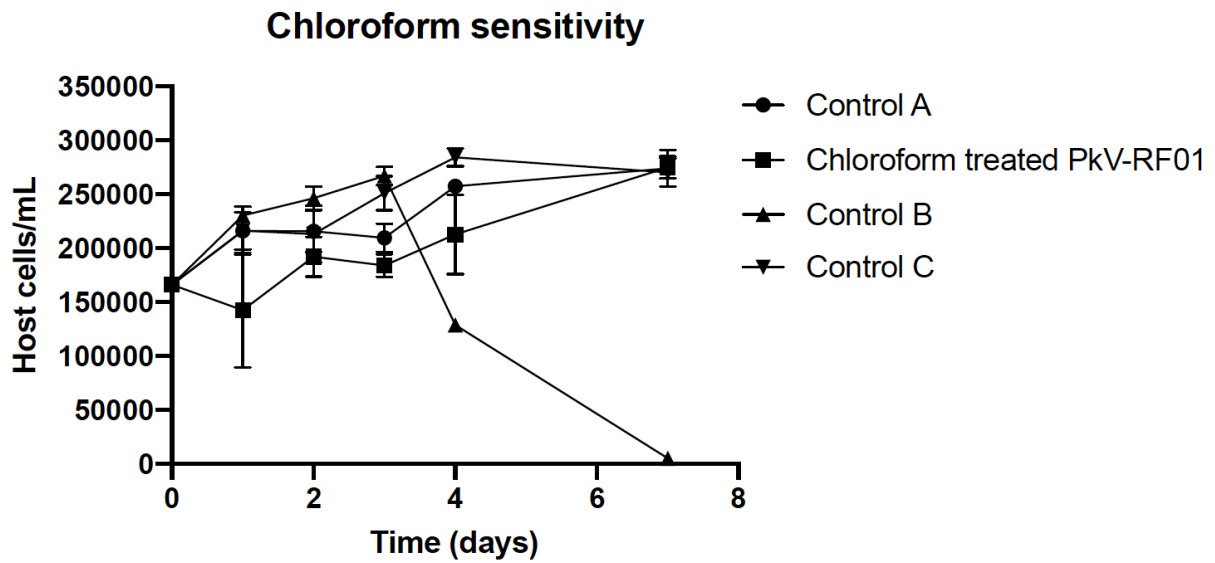
290 In addition to encoding the two aaRSs reported in the main text, we found that PkV  
291 RF01 encodes a catalytic domain for Asn/Asp-RNA<sub>t</sub> (ORF762) also found in  
292 Prochlorococcus phages P-SSM2, 5, and 7. PkV RF01 encodes other translation-related  
293 proteins also present in other *Mimiviridae*, namely, the translation initiation factor 4F cap  
294 binding subunit (eIF-4E; ORF 512), the helicase subunit (eIF-4A; ORF 229), and the peptide  
295 chain release factor 1 (eRF1; ORF 651). The latter protein is not orthologous to chain release  
296 factors in other *Mimiviridae*, as it exhibits much higher sequence conservation with cellular or  
297 even *Marseilleviridae* homologs. PkV RF01 shares with PgV the translation elongation factor  
298 eEF3 (ORF 489), whose sequence in both viral species is highly similar to haptophyte  
299 homologs. In addition, PkV RF01 encodes the translation elongation factor EF-1alpha  
300 (ORF946) that is absent in other *Mimiviridae* members but present in AaV. EF-1alpha of PkV  
301 RF01 was most likely acquired from haptophytes, as it has a high amino acid identity (57%)  
302 to that of *E. huxleyi*, whereas the AaV homolog is most closely related (62% aa identity) to that  
303 of diatoms. PkV RF01 also encodes the translation initiation factor 1A (EIF1A) (ORF 62)  
304 with no detectable homolog in viruses ( $E$ -value =  $1 \times 10^{-5}$  in BLASTP searches against the  
305 Virus-Host DB database). While translation-associated genes may predate the divergence of  
306 known extant eukaryotic lineages, the above examples demonstrate that some other genes  
307 were acquired much more recently, consistent with the “accordion model” of episodic gain  
308 and loss of genes in the evolution of these viruses (15, 50).

### 309 **Other carbohydrate-active enzymes**

310 Other carbohydrate-active enzymes in the PkV RF01 genome include seven glycoside  
311 hydrolases (GHs), four carbohydrate esterases (CEs), one polysaccharide lyase (PL), one  
312 carbohydrate-binding module (CBM), and a putative sugar fermentation stimulation protein A  
313 (ORF 1003) possibly involved in maltose metabolism. These numbers are not excessively  
314 high compared with other viruses. Other detected ORFs were homologous to enzymes  
315 involved in carbohydrate transport and metabolism, notably a transketolase (ORF 528)  
316 involved in the pentose phosphate pathway in all organisms and in the Calvin cycle of  
317 photosynthetic organisms. Finally, we detected a 6-phosphofructo-2-kinase/fructose-2,6-  
318 biphosphatase 2 (ORF 539) and a mannose-1-phosphate guanylyltransferase/mannose-6-  
319 phosphate isomerase (ORF 836) respectively involved in fructose and mannose metabolism.

320 **Figures**

321



322

323 **Fig. S1. Reduction of PkV RF01 infectivity with chloroform.**

324 Experiments were set up in triplicate, and host cells were counted by flow cytometry.

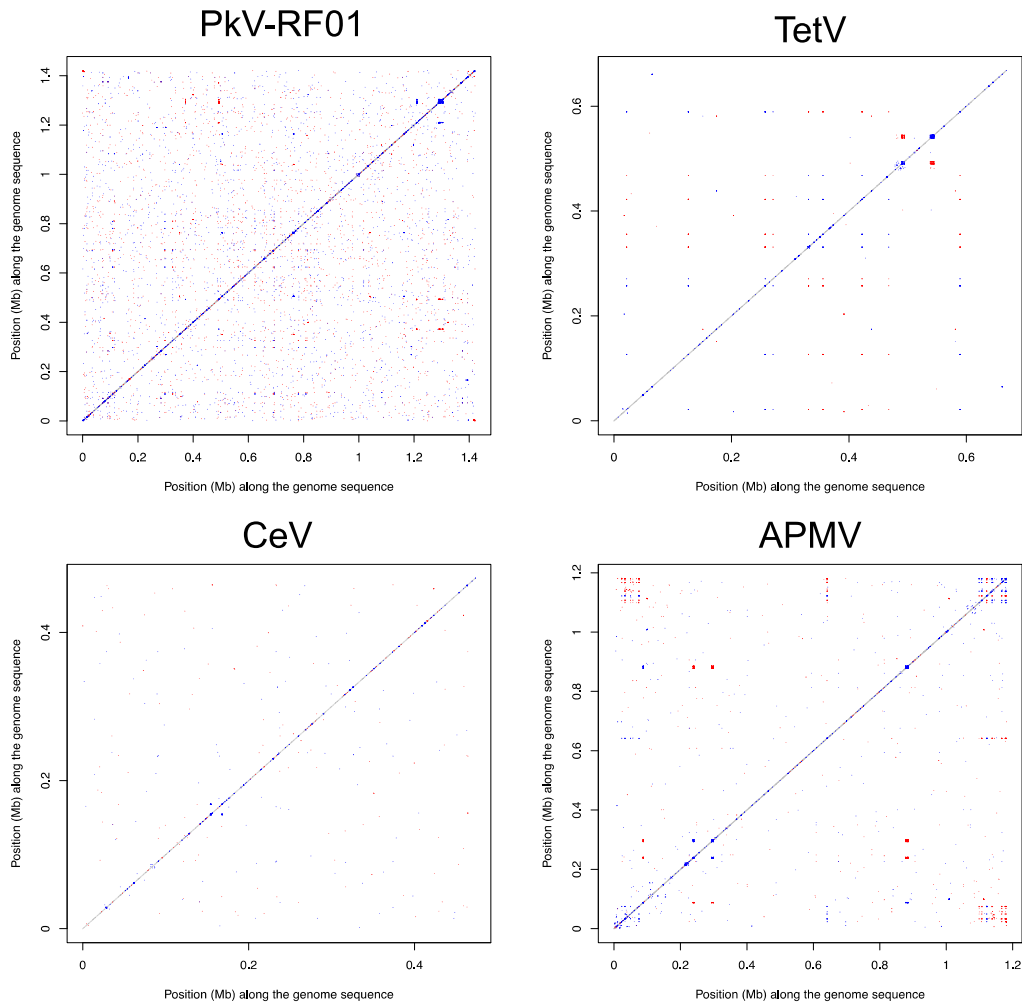
325 Chloroform-treated PkV RF01 was added to exponentially growing He UiO028 cells in a 1:10

326 volume ratio. Controls were He UiO028 cells incubated with chloroform-treated medium

327 (Control A), untreated PkV RF01 (Control B), and untreated medium (Control C). SDs are

328 indicated with error bars.

329

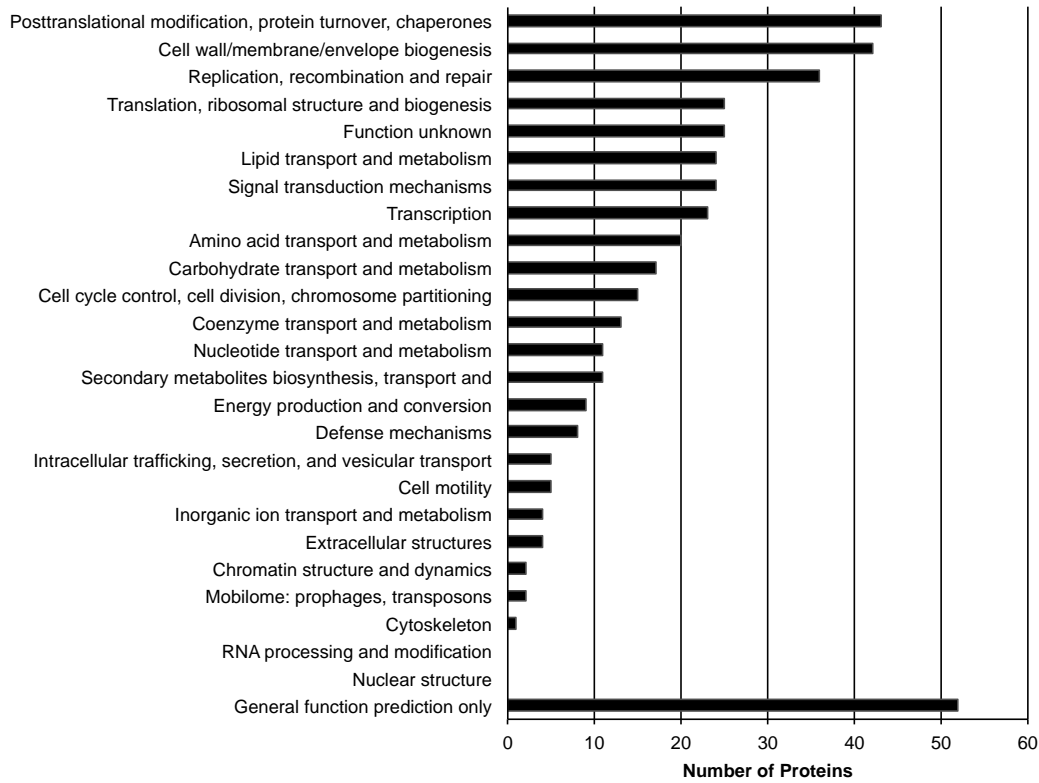


330

331

332 **Fig. S2. High density of exact small repeats in the PkV RF01 genome.**

333 Dot plots show exact direct (blue) or inverted (red) genomic repeats of at least 20 nucleotides  
334 in PkV RF01, another unclassified *Mimiviridae* (TetV), a member of “Mesomimivirinae”  
335 (CeV), and a “Megavirinae” member (APMV). Self-alignments were removed.

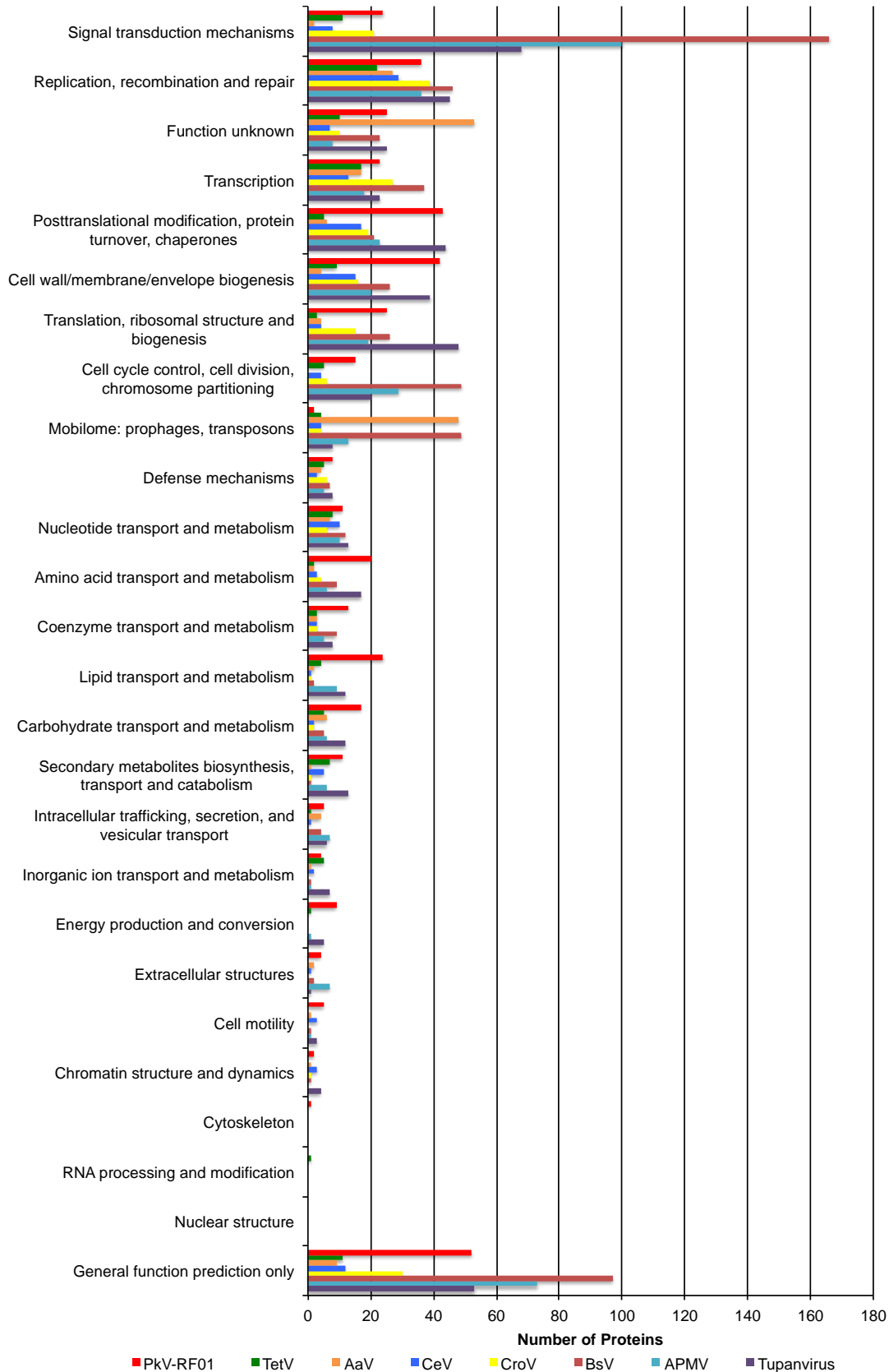


336

337 **Fig. S3. COG functional distribution of 339 proteins encoded by PkV RF01.**

338



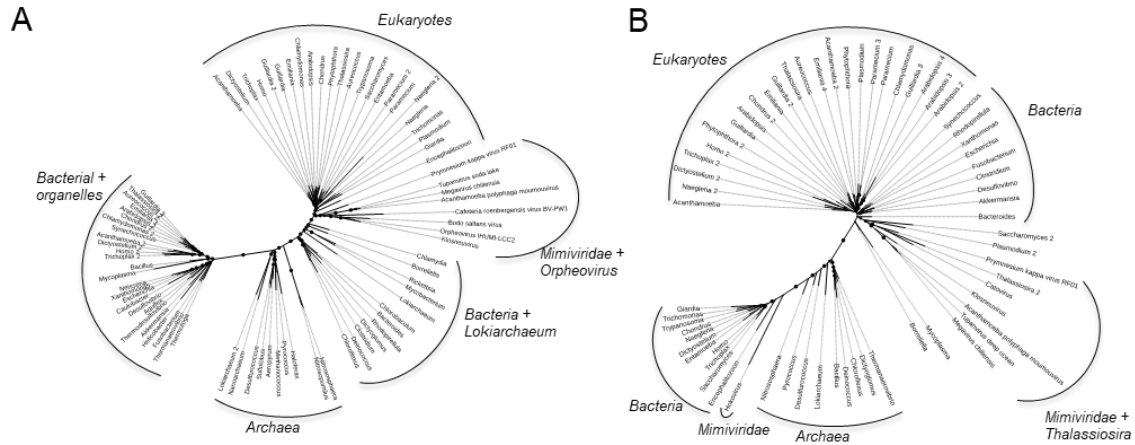


339

340 **Fig. S4. Comparative COG functional distribution among *Mimiviridae* members.**

341 COG sequences were automatically searched against the proteomes of each virus using

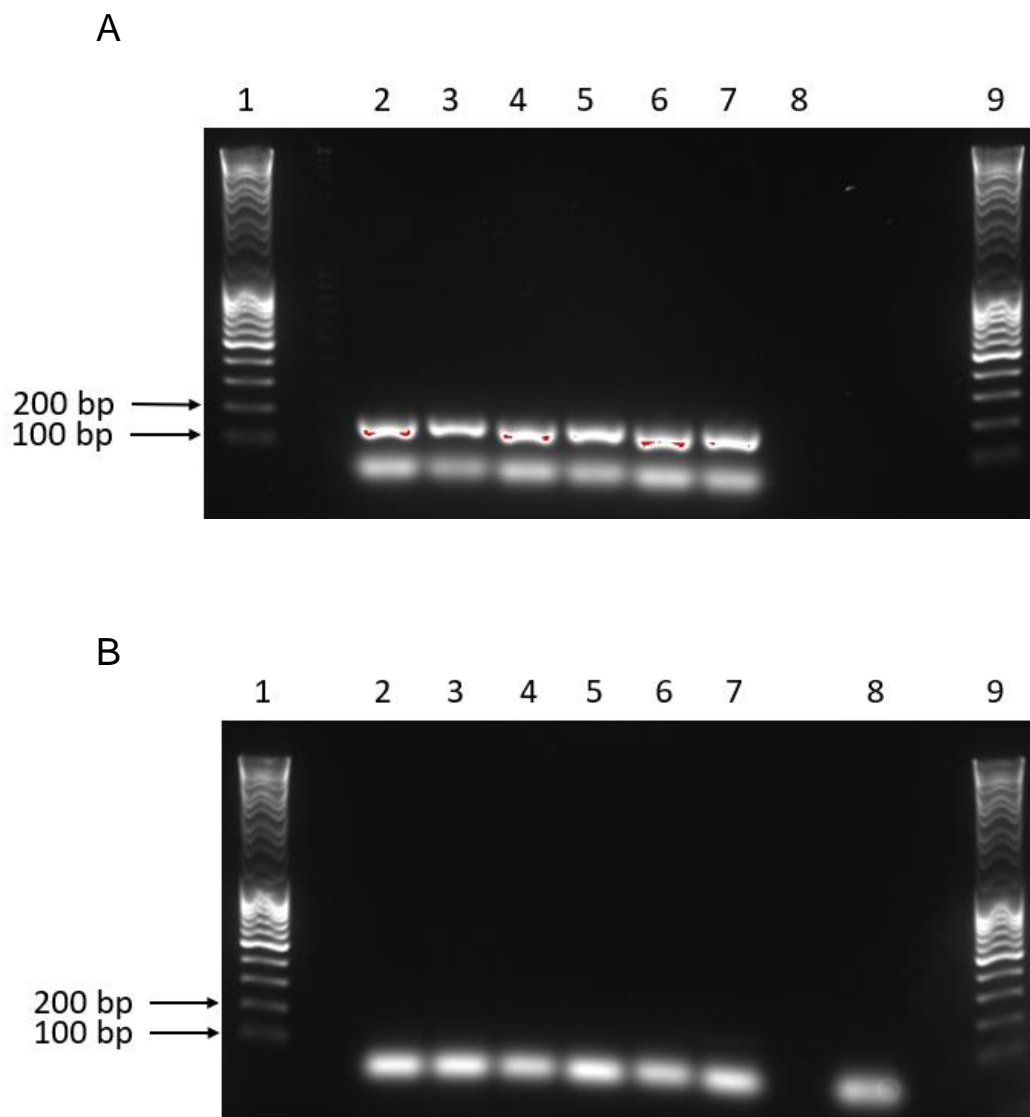
342 BLASTP with an  $E$ -value of  $1 \times 10^{-5}$  as the significant similarity threshold.



343

344 **Fig. S5. Bayesian phylogenetic trees of two viral amino-acyl tRNA synthetases**  
345 **and their cellular homologs.**

346 (A) Isoleucine tRNA synthetases. (B) Aspartyl tRNA synthetases. Branches supported by  
347 posterior probability (PP) values >70% are indicated by circles whose diameters are  
348 proportional to the PP value.

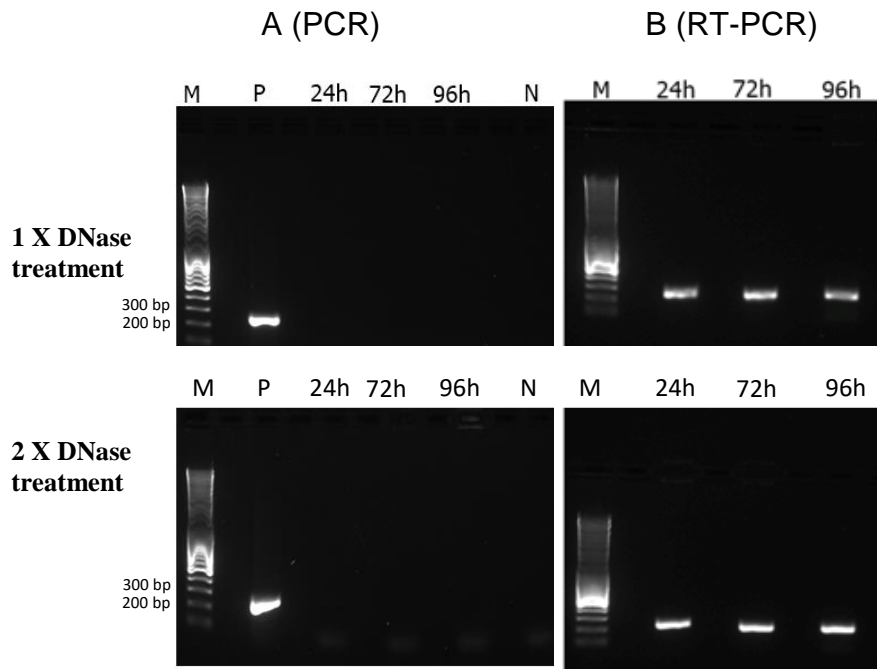


349

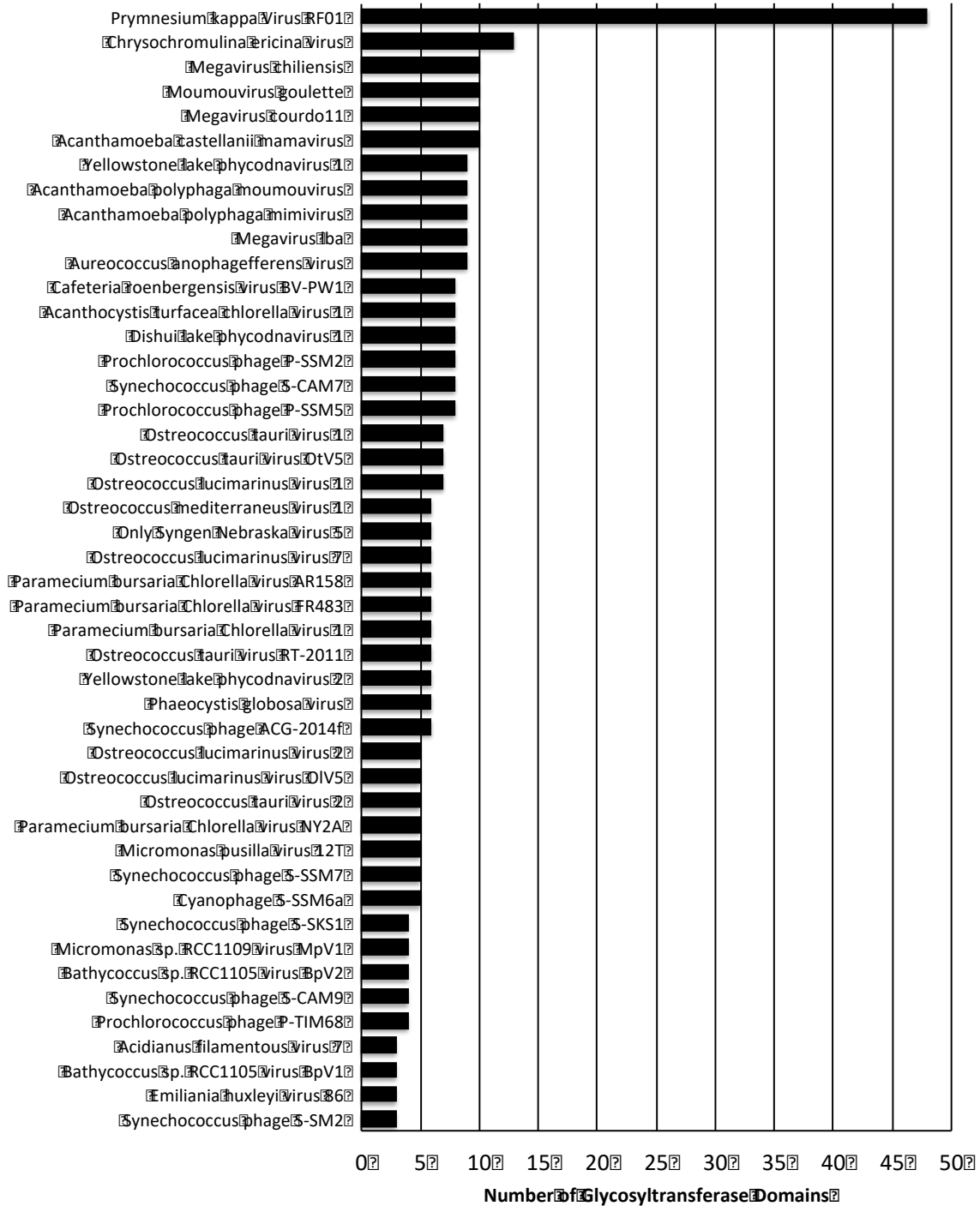
350 **Fig. S6. PCR optimization and confirmation of the *SDHA* gene in the PkV RF01**  
351 **genome.**

352 (A–B) Results of PCR with *SDHA* primers using genomic PkV RF01 DNA (A) and genomic  
353 He UiO028 DNA (B) as templates. Lanes 1 and 9, DNA ladder; 2–7, optimization of the PCR  
354 annealing temperature from 55°C (2) to 60°C (7); 8, negative control (sdH<sub>2</sub>O).

355



356 **Fig. S7. PCR and RT-PCR optimization using an internal control gene (*mcp*).**  
357 PCR and RT-PCR were carried out after removal of genomic DNA using a TURBO DNA-free  
358 kit. Samples were taken 24, 72, and 96 h after infection. Two different protocols, both  
359 provided in the TURBO DNA-free kit manual, were used to optimize the reactions. (A) PCR  
360 check for the presence of genomic DNA after RNA isolation treated with 1x and 2x DNase,  
361 in the upper and lower panels respectively. P, positive control (PkV RF01 genomic DNA); N,  
362 negative control (sdH<sub>2</sub>O). (B) Result of RT-PCR of samples harvested 24, 72 and 96 h post  
363 infection. M, DNA marker (MassRuler DNA Ladder Mix, Thermo Fisher, 80 to 10,000 bp).



364

365 **Fig. S8. Comparative distribution of glycosyltransferase domains among viruses.**

366 **Tables**

367 **Table S1. Type and position of 40 predicted tRNA genes in the PkV RF01 genome**  
 368

Anti codon	Begin	End	Strand
CAT	3556	3483	-
NNN	90515	90393	-
AGT	165083	165153	+
TAT	165371	165444	+
TAA	165508	165590	+
TTT	165592	165666	+
TTT	165672	165744	+
CAT	165763	165835	+
GTT	165838	165911	+
TTG	166072	166144	+
AAT	166165	166238	+
TGT	686381	686452	+
GCT	787944	787863	-
TGA	930076	930157	+
TGC	941356	941284	-
TGG	956727	956656	-
TCC	956801	956731	-
AAT	1342428	1342564	+
CAA	1388099	1388180	+
CAT	1388185	1388257	+
GTT	1388263	1388336	+
TTG	1388494	1388565	+
CTT	1388664	1388736	+
CTT	1388946	1389018	+
TCT	1389231	1389303	+
TCT	1389516	1389588	+
TCT	1389801	1389873	+
CTT	1390089	1390163	+
TCT	1393421	1393493	+
TTC	1393523	1393594	+
CAA	1393697	1393778	+
TAT	1393782	1393855	+
TAA	1393963	1394044	+
TAT	1394048	1394121	+
TAA	1394229	1394310	+
TAT	1394314	1394387	+
TAA	1394495	1394576	+
TAT	1394580	1394653	+
TAA	1394761	1394841	+
CAT	1417619	1417692	+

369  
370

371 The distribution of tRNA types is as follows: tRNA<sub>Ile</sub> and tRNA<sub>Leu</sub>, seven each; tRNA<sub>Lys</sub>,  
 372 five; tRNA<sub>Arg</sub> and tRNA<sub>Met</sub>, four each; tRNA<sub>Asn</sub>, tRNA<sub>Gln</sub>, tRNA<sub>Ser</sub>, and tRNA<sub>Thr</sub>, two each;  
 373 and tRNA<sub>Ala</sub>, tRNA<sub>Glu</sub>, tRNA<sub>Gly</sub>, tRNA<sub>Pro</sub>, and undetermined, one each.



374 **Table S2. Genes related to lipid metabolism**

ORF	Length (aa)	Annotation	KEGG orthology	Pathway
ORF30	276	2,4-dienoyl-CoA reductase, mitochondrial [EC:1.3.1.34]	K13236	Beta oxidation
ORF33	888	Putative CoA-transferase	no significant hit	Beta oxidation
ORF121	225	glycerophosphoryl diester phosphodiesterase	K01126	Glycerophospholipids metabolisms
ORF138	2116	Fatty acid synthase (FASN)	K00665	Fatty acid biosynthesis
ORF142	523	Long-chain-fatty-acid--CoA ligase ACSBG [EC:6.2.1.3]	K15013	Fatty acid degradation /biosynthesis / Beta Oxidation
ORF175	1303	Acetyl-CoA carboxylase / biotin carboxylase 1 [EC:6.4.1.2 6.3.4.14 2.1.3.15]	K11262	Fatty acid biosynthesis
ORF236	410	Glutaryl-CoA dehydrogenase [EC:1.3.8.6]	K00252	Fatty acid degradation
ORF293	330	Lysophospholipase like	no significant hit	not assigned
ORF357	313	Lysophospholipase like	no significant hit	not assigned
ORF386	293	Triacylglycerol lipase [EC:3.1.1.3]	K01046	Glycerolipid metabolism
ORF481	503	Lipase like	no significant hit	not assigned
ORF635	282	Lipase-like	no significant hit	not assigned
ORF653	292	Lipase-like	no significant hit	not assigned
ORF690	260	Lipase-like	no significant hit	not assigned
ORF774	327	Lysophospholipid Acyltransferases [EC:2.3.1.22]	K14457	Glycerolipid metabolism
ORF694	336	Lipase esterase (Carbohydrate esterase CE10)	no significant hit	not assigned
ORF695	335	Lipase esterase (Carbohydrate esterase CE10)	no significant hit	not assigned
ORF886	516	Stearoyl-CoA desaturase (Delta-9 desaturase) [EC:1.14.19.1]	K00507	Biosynthesis of unsaturated fatty acids
ORF902	2083	Fatty acid synthase (FASN)	K00665	Fatty acid biosynthesis
ORF904	678	Long-chain-fatty-acid--CoA ligase ACSBG [EC:6.2.1.3]	K15013	Fatty acid degradation /biosynthesis / Beta Oxidation
ORF1016	422	Cyclopropane-fatty-acyl-phospholipid synthase [EC:2.1.1.79]	k00574	not assigned
ORF1046	652	Acyl-CoA dehydrogenase	K06445	Fatty acid degradation / Beta oxidation

\*ORF138 and ORF902 share 2% aa identity  
 \*\*ORF142 and ORF904 share 2% aa identity  
 \*\*\*ORF694 and ORF695 share 2% aa identity

375

376 **Table S3. Details for tree reconstruction**

Protein	Burn-in	Sub-sampling	Chai n	#Trees	Maxdiff	Meandiff
Five NCLDV-core proteins*	2000	2	1	16,680	0.32	0.006
			3	16,725		
			4	16,483		
			2	16,430		
Rpb2	Reconstructed using FastTree v2.1 default settings					
SDHA	Reconstructed using RaxML					
SDHB	Reconstructed using RaxML					
AsnRS	10,000	3	1	15,485	0.27	0.02
			2	15,066		
			3	15,627		
IleRS	10,000	3	1	10,757	0.16	0.009
			2	10,819		
			3	10,856		

377 \* D5-like helicase-primase (NCVOG0023), DNA polymerase elongation subunit family B (NCVOG0038),  
 378 DNA or RNA helicases of superfamily II (NCVOG0076), packaging ATPase (NCVOG0249), and Poxvirus Late  
 379 Transcription Factor VLTF3 like (NCVOG0262).  
 380

381 **Table S4. Forward and reverse PCR primers for amplification of *vSDHA* and**  
 382 ***MCP***

Primer name	Sequence (5' - 3')	PCR product (bp)
<i>vSDHA</i> -F1	ATGTGCCGAGAAGCTCCTAA	154
<i>vSDHA</i> -R1	CTGCACAGGCTGTTTCGATAA	
PkV-RF01-MCP-F	GATGAACCTTGCCCACT	256
PkV-RF01-MCP-F	GTGCATGGTACGTTTTCGTG	

383

## 384 **References**

385

- 386 1. Marie D, Brussaard CPD, Thyraug R, Bratbak G, Vaultot D. 1999. Enumeration of  
387 Marine Viruses in Culture and Natural Samples by Flow Cytometry. *Appl Environ*  
388 *Microbiol* 65:45–52.
- 389 2. Brussaard CPD. 2004. Optimization of procedures for counting viruses by flow  
390 cytometry. *Appl Environ Microbiol* 70:1506–1513.
- 391 3. Johannessen TV, Bratbak G, Larsen A, Ogata H, Egge ES, Edvardsen B, Eikrem W,  
392 Sandaa R-A. 2015. Characterisation of three novel giant viruses reveals huge diversity  
393 among viruses infecting Prymnesiales (Haptophyta). *Virology* 476:180–188.
- 394 4. Jarvis B, Wilrich C, Wilrich P-T. 2010. Reconsideration of the derivation of Most  
395 Probable Numbers, their standard deviations, confidence bounds and rarity values. *J*  
396 *Appl Microbiol* 109:1660–1667.
- 397 5. Kremer JR, Mastrorade DN, McIntosh JR. 1996. Computer visualization of three-  
398 dimensional image data using IMOD. *J Struct Biol* 116:71–76.
- 399 6. Lawrence JE, Steward GF. 2010. Purification of viruses by centrifugation, p. 166–181.  
400 *In* Wilhelm, S, Weinbauer, M, Suttle, C (eds.), *Manual of Aquatic Viral Ecology*.  
401 American Society of Limnology and Oceanography.
- 402 7. Sandaa R-A, E. Storesund J, Olesin E, Lund Paulsen M, Larsen A, Bratbak G, Ray JL.  
403 2018. Seasonality Drives Microbial Community Structure, Shaping both Eukaryotic and  
404 Prokaryotic Host–Viral Relationships in an Arctic Marine Ecosystem. *Viruses* 10.
- 405 8. Margulies M, Egholm M, Altman WE, Attiya S, Bader JS, Bemben LA, Berka J,  
406 Braverman MS, Chen Y-J, Chen Z, Dewell SB, Du L, Fierro JM, Gomes XV, Godwin  
407 BC, He W, Helgesen S, Ho CH, Irzyk GP, Jando SC, Alenquer MLI, Jarvie TP, Jirage  
408 KB, Kim J-B, Knight JR, Lanza JR, Leamon JH, Lefkowitz SM, Lei M, Li J, Lohman  
409 KL, Lu H, Makhijani VB, McDade KE, McKenna MP, Myers EW, Nickerson E, Nobile  
410 JR, Plant R, Puc BP, Ronan MT, Roth GT, Sarkis GJ, Simons JF, Simpson JW,  
411 Srinivasan M, Tartaro KR, Tomasz A, Vogt KA, Volkmer GA, Wang SH, Wang Y,  
412 Weiner MP, Yu P, Begley RF, Rothberg JM. 2005. Genome sequencing in  
413 microfabricated high-density picolitre reactors. *Nature* 437:376–380.
- 414 9. Gordon D, Green P. 2013. Consed: a graphical editor for next-generation sequencing.  
415 *Bioinformatics* 29:2936–2937.
- 416 10. Loman NJ, Quick J, Simpson JT. 2015. A complete bacterial genome assembled de novo  
417 using only nanopore sequencing data. *Nat Methods* 12:733–735.
- 418 11. Walker BJ, Abeel T, Shea T, Priest M, Abouelliel A, Sakthikumar S, Cuomo CA, Zeng  
419 Q, Wortman J, Young SK, Earl AM. 2014. Pilon: An Integrated Tool for Comprehensive  
420 Microbial Variant Detection and Genome Assembly Improvement. *PLOS ONE*  
421 9:e112963.

- 422 12. Yutin N, Wolf YI, Raoult D, Koonin EV. 2009. Eukaryotic large nucleo-cytoplasmic  
423 DNA viruses: Clusters of orthologous genes and reconstruction of viral genome  
424 evolution. *Virology* 6:223.
- 425 13. Yutin N, Wolf YI, Koonin EV. 2014. Origin of giant viruses from smaller DNA viruses  
426 not from a fourth domain of cellular life. *Virology* 466–467:38–52.
- 427 14. Eddy SR. 2011. Accelerated Profile HMM Searches. *PLOS Comput Biol* 7:e1002195.
- 428 15. Schulz F, Yutin N, Ivanova NN, Ortega DR, Lee TK, Vierheilig J, Daims H, Horn M,  
429 Wagner M, Jensen GJ, Kyrpides NC, Koonin EV, Woyke T. 2017. Giant viruses with an  
430 expanded complement of translation system components. *Science* 356:82–85.
- 431 16. Katoh K, Standley DM. 2013. MAFFT multiple sequence alignment software version 7:  
432 improvements in performance and usability. *Mol Biol Evol* 30:772–780.
- 433 17. Capella-Gutiérrez S, Silla-Martínez JM, Gabaldón T. 2009. trimAl: a tool for automated  
434 alignment trimming in large-scale phylogenetic analyses. *Bioinforma Oxf Engl*  
435 25:1972–1973.
- 436 18. Lartillot N, Lepage T, Blanquart S. 2009. PhyloBayes 3: a Bayesian software package  
437 for phylogenetic reconstruction and molecular dating. *Bioinformatics* 25:2286–2288.
- 438 19. Stamatakis A. 2014. RAxML version 8: a tool for phylogenetic analysis and post-  
439 analysis of large phylogenies. *Bioinforma Oxf Engl* 30:1312–1313.
- 440 20. Letunic I, Bork P. 2016. Interactive tree of life (iTOL) v3: an online tool for the display  
441 and annotation of phylogenetic and other trees. *Nucleic Acids Res* 44:W242–W245.
- 442 21. Price MN, Dehal PS, Arkin AP. 2009. FastTree: Computing Large Minimum Evolution  
443 Trees with Profiles instead of a Distance Matrix. *Mol Biol Evol* 26:1641–1650.
- 444 22. Lartillot N, Rodrigue N, Stubbs D, Richer J. 2013. PhyloBayes MPI: phylogenetic  
445 reconstruction with infinite mixtures of profiles in a parallel environment. *Syst Biol*  
446 62:611–615.
- 447 23. Lartillot N, Philippe H. 2004. A Bayesian Mixture Model for Across-Site  
448 Heterogeneities in the Amino-Acid Replacement Process. *Mol Biol Evol* 21:1095–1109.
- 449 24. Besemer J, Lomsadze A, Borodovsky M. 2001. GeneMarkS: a self-training method for  
450 prediction of gene starts in microbial genomes. Implications for finding sequence motifs  
451 in regulatory regions. *Nucleic Acids Res* 29:2607–2618.
- 452 25. Lowe TM, Chan PP. 2016. tRNAscan-SE On-line: integrating search and context for  
453 analysis of transfer RNA genes. *Nucleic Acids Res* 44:W54–57.
- 454 26. Mihara T, Nishimura Y, Shimizu Y, Nishiyama H, Yoshikawa G, Uehara H, Hingamp P,  
455 Goto S, Ogata H. 2016. Linking Virus Genomes with Host Taxonomy. *Viruses* 8:66.
- 456 27. Pruitt KD, Tatusova T, Maglott DR. 2007. NCBI reference sequences (RefSeq): a  
457 curated non-redundant sequence database of genomes, transcripts and proteins. *Nucleic*  
458 *Acids Res* 35:D61–D65.

- 459 28. Suzek BE, Wang Y, Huang H, McGarvey PB, Wu CH. 2015. UniRef clusters: a  
460 comprehensive and scalable alternative for improving sequence similarity searches.  
461 *Bioinformatics* 31:926–932.
- 462 29. Tatusov RL, Galperin MY, Natale DA, Koonin EV. 2000. The COG database: a tool for  
463 genome-scale analysis of protein functions and evolution. *Nucleic Acids Res* 28:33–36.
- 464 30. Marchler-Bauer A, Derbyshire MK, Gonzales NR, Lu S, Chitsaz F, Geer LY, Geer RC,  
465 He J, Gwadz M, Hurwitz DI, Lanczycki CJ, Lu F, Marchler GH, Song JS, Thanki N,  
466 Wang Z, Yamashita RA, Zhang D, Zheng C, Bryant SH. 2015. CDD: NCBI’s conserved  
467 domain database. *Nucleic Acids Res* 43:D222–D226.
- 468 31. Kanehisa M, Sato Y, Kawashima M, Furumichi M, Tanabe M. 2016. KEGG as a  
469 reference resource for gene and protein annotation. *Nucleic Acids Res* 44:D457–D462.
- 470 32. Zhang H, Yohe T, Huang L, Entwistle S, Wu P, Yang Z, Busk PK, Xu Y, Yin Y. 2018.  
471 dbCAN2: a meta server for automated carbohydrate-active enzyme annotation. *Nucleic*  
472 *Acids Res* 46:W95–W101.
- 473 33. Emms DM, Kelly S. 2015. OrthoFinder: solving fundamental biases in whole genome  
474 comparisons dramatically improves orthogroup inference accuracy. *Genome Biol*  
475 16:157.
- 476 34. Zimmermann L, Stephens A, Nam S-Z, Rau D, Kübler J, Lozajic M, Gabler F, Söding J,  
477 Lupas AN, Alva V. 2018. A Completely Reimplemented MPI Bioinformatics Toolkit  
478 with a New HHpred Server at its Core. *J Mol Biol* 430:2237–2243.
- 479 35. Sunagawa S, Coelho LP, Chaffron S, Kultima JR, Labadie K, Salazar G, Djahanschiri B,  
480 Zeller G, Mende DR, Alberti A, Cornejo-Castillo FM, Costea PI, Cruaud C, d’Ovidio F,  
481 Engelen S, Ferrera I, Gasol JM, Guidi L, Hildebrand F, Kokoszka F, Lepoivre C, Lima-  
482 Mendez G, Poulain J, Poulos BT, Royo-Llonch M, Sarmiento H, Vieira-Silva S, Dimier  
483 C, Picheral M, Searson S, Kandels-Lewis S, Tara Oceans coordinators, Bowler C, de  
484 Vargas C, Gorsky G, Grimsley N, Hingamp P, Iudicone D, Jaillon O, Not F, Ogata H,  
485 Pesant S, Speich S, Stemmann L, Sullivan MB, Weissenbach J, Wincker P, Karsenti E,  
486 Raes J, Acinas SG, Bork P. 2015. Ocean plankton. Structure and function of the global  
487 ocean microbiome. *Science* 348:1261359.
- 488 36. Villar E, Vannier T, Vernet C, Lescot M, Cuenca M, Alexandre A, Bachelerie P,  
489 Rosnet T, Pelletier E, Sunagawa S, Hingamp P. 2018. The Ocean Gene Atlas: exploring  
490 the biogeography of plankton genes online. *Nucleic Acids Res* 46:W289–W295.
- 491 37. El-Gebali S, Mistry J, Bateman A, Eddy SR, Luciani A, Potter SC, Qureshi M,  
492 Richardson LJ, Salazar GA, Smart A, Sonnhammer ELL, Hirsh L, Paladin L, Piovesan  
493 D, Tosatto SCE, Finn RD. 2019. The Pfam protein families database in 2019. *Nucleic*  
494 *Acids Res* 47:D427–D432.
- 495 38. Eddy SR. 1998. Profile hidden Markov models. *Bioinformatics* 14:755–763.
- 496 39. Carradec Q, Pelletier E, Silva CD, Alberti A, Seeleuthner Y, Blanc-Mathieu R, Lima-  
497 Mendez G, Rocha F, Tirichine L, Labadie K, Kirilovsky A, Bertrand A, Engelen S,  
498 Madoui M-A, Méheust R, Poulain J, Romac S, Richter DJ, Yoshikawa G, Dimier C,  
499 Kandels-Lewis S, Picheral M, Searson S, Jaillon O, Aury J-M, Karsenti E, Sullivan MB,

- 500 Sunagawa S, Bork P, Not F, Hingamp P, Raes J, Guidi L, Ogata H, Vargas C de,  
501 Iudicone D, Bowler C, Wincker P. 2018. A global ocean atlas of eukaryotic genes. *Nat*  
502 *Commun* 9:373.
- 503 40. Keeling PJ, Burki F, Wilcox HM, Allam B, Allen EE, Amaral-Zettler LA, Armbrust EV,  
504 Archibald JM, Bharti AK, Bell CJ, Beszteri B, Bidle KD, Cameron CT, Campbell L,  
505 Caron DA, Cattolico RA, Collier JL, Coyne K, Davy SK, Deschamps P, Dyhrman ST,  
506 Edvardsen B, Gates RD, Gobler CJ, Greenwood SJ, Guida SM, Jacobi JL, Jakobsen KS,  
507 James ER, Jenkins B, John U, Johnson MD, Juhl AR, Kamp A, Katz LA, Kiene R,  
508 Kudryavtsev A, Leander BS, Lin S, Lovejoy C, Lynn D, Marchetti A, McManus G,  
509 Nedelcu AM, Menden-Deuer S, Miceli C, Mock T, Montresor M, Moran MA, Murray S,  
510 Nadathur G, Nagai S, Ngam PB, Palenik B, Pawlowski J, Petroni G, Piganeau G,  
511 Posewitz MC, Rengefors K, Romano G, Rumpho ME, Rynearson T, Schilling KB,  
512 Schroeder DC, Simpson AGB, Slamovits CH, Smith DR, Smith GJ, Smith SR, Sosik  
513 HM, Stief P, Theriot E, Twary SN, Umale PE, Vaultot D, Wawrik B, Wheeler GL,  
514 Wilson WH, Xu Y, Zingone A, Worden AZ. 2014. The Marine Microbial Eukaryote  
515 Transcriptome Sequencing Project (MMETSP): Illuminating the Functional Diversity of  
516 Eukaryotic Life in the Oceans through Transcriptome Sequencing. *PLOS Biol*  
517 12:e1001889.
- 518 41. Buchfink B, Xie C, Huson DH. 2015. Fast and sensitive protein alignment using  
519 DIAMOND. *Nat Methods* 12:59–60.
- 520 42. Redrejo-Rodríguez M, Salas ML. 2014. Repair of base damage and genome  
521 maintenance in the nucleo-cytoplasmic large DNA viruses. *Virus Res* 179:12–25.
- 522 43. Blanc-Mathieu R, Ogata H. 2016. DNA repair genes in the Megavirales pangenome.  
523 *Curr Opin Microbiol* 31:94–100.
- 524 44. Keto-Timonen R, Hietala N, Palonen E, Hakakorpi A, Lindström M, Korkeala H. 2016.  
525 Cold Shock Proteins: A Minireview with Special Emphasis on Csp-family of  
526 Enteropathogenic *Yersinia*. *Front Microbiol* 7.
- 527 45. Wolf YI, Aravind L, Grishin NV, Koonin EV. 1999. Evolution of Aminoacyl-tRNA  
528 Synthetases—Analysis of Unique Domain Architectures and Phylogenetic Trees Reveals  
529 a Complex History of Horizontal Gene Transfer Events. *Genome Res* 9:689–710.
- 530 46. Cvetesic N, Dulic M, Bilus M, Sostaric N, Lenhard B, Gruic-Sovulj I. 2016. Naturally  
531 Occurring Isoleucyl-tRNA Synthetase without tRNA-dependent Pre-transfer Editing. *J*  
532 *Biol Chem* 291:8618–8631.
- 533 47. Felsenstein J. 1978. Cases in which Parsimony or Compatibility Methods Will be  
534 Positively Misleading. *Syst Zool* 27:401–410.
- 535 48. Moreira D, López-García P. 2015. Evolution of viruses and cells: do we need a fourth  
536 domain of life to explain the origin of eukaryotes? *Philos Trans R Soc B Biol Sci* 370.
- 537 49. Lartillot N, Brinkmann H, Philippe H. 2007. Suppression of long-branch attraction  
538 artefacts in the animal phylogeny using a site-heterogeneous model. *BMC Evol Biol*  
539 7:S4.

540 50. Filée J. 2015. Genomic comparison of closely related Giant Viruses supports an  
541 accordion-like model of evolution. *Front Microbiol* 6.

542